Neodymium isotopic composition and concentration in the western North Atlantic Ocean: results from the GEOTRACES GA02 section

Myriam Lambelet[a*], Tina van de Flierdt[a], Kirsty Crocket[b], Mark Rehkämper[a], Katharina Kreissig[a], Barry Coles[a], Micha J A Rijkenberg[c], Loes J A Gerringa[c], Hein J W de Baar[c], Reiner Steinfeldt[d]

[a] Department of Earth Science and Engineering, Imperial College London, SW7 2BP, UK

[b] The Scottish Association for Marine Science, Scottish Marine Institute, Oban Argyll PA37 1QA, UK

[c] Royal Netherlands Institute for Sea Research (Royal NIOZ), 1790 AB Den Burg, the Netherlands

[d] Department of Oceanography, University of Bremen, 28334 Bremen, Germany

* Corresponding author: m.lambelet@imperial.ac.uk; 0044 20 7594 7332

Abstract

The neodymium (Nd) isotopic composition of seawater is commonly used as a proxy to study past changes in the thermohaline circulation. The modern database for such reconstructions is however poor and the understanding of the underlying processes is incomplete. Here we present new observational data for Nd isotopes and concentrations from twelve seawater depth profiles, which follow the flow path of North Atlantic Deep Water (NADW) from its formation region in the North Atlantic to the northern equatorial Atlantic. Samples were collected during two cruises constituting the northern part of the Dutch GEOTRACES transect GA02 in 2010. The results show that the different water masses in the subpolar North Atlantic Ocean, which ultimately constitute NADW, have the following Nd isotope characteristics: Upper Labrador Sea Water (ULSW), ε_{Nd} = -14.2 ± 0.3; Labrador Sea Water (LSW), ε_{Nd} = -13.7 ± 0.9; Northeast Atlantic Deep Water (NEADW), ε_{Nd} = -12.5 ± 0.6; Northwest Atlantic Bottom Water (NWABW), ε_{Nd} = -11.8 ± 1.4. In the subtropics, where these source water masses have mixed to form NADW, which is exported to the global ocean, upper-NADW is characterised by ε_{Nd} values of -13.2 ± 1.0 (2sd) and lower-NADW exhibits values of ε_{Nd} = -12.4 ± 0.4 (2sd). While both signatures overlap within error, the signature for lower-NADW is significantly more radiogenic than the traditionally used value for NADW (ε_{Nd} = -13.5) due to the dominance of source waters from the Nordic Seas (NWABW and NEADW). Comparison between the concentration profiles and the corresponding Nd isotope profiles with other water mass properties such as salinity, silicate concentrations, neutral densities and chlorofluorocarbon (CFC) concentration provides novel insights into the geochemical cycle of Nd and reveals that different processes are necessary to account for the observed Nd characteristics in the subpolar and subtropical gyres and throughout the vertical water column. While our data set provides additional insights into

43 the contribution of boundary exchange in areas of sediment resuspension, the results for
44 open ocean seawater demonstrate, at an unprecedented level, the suitability of Nd isotopes
45 to trace modern water masses in the strongly advecting western Atlantic Ocean.

46 **1. Introduction**

47 Ocean circulation has an important role in modulating global heat transport and the
48 carbon cycle, two key players in understanding climate change now and in the past
49 (Broecker, 1991; Ganachaud and Wunsch, 2000; Rahmstorf, 2002; Alley et al., 2003;
50 Marshall and Speer, 2012). While tracing modern water masses is traditionally achieved
51 using physical properties and nutrient contents, tracing water bodies back in time remains
52 more challenging (e.g. Lynch-Stieglitz et al., 2007; Adkins, 2013).

53 One proxy that has been developed over the past ~35 years as a 'quasi-conservative'
54 tracer of ocean circulation are neodymium (Nd) isotopes (see reviews by Frank (2002),
55 Goldstein and Hemming (2003) and van de Flierdt and Frank (2010)). The terminology 'quasi-
56 conservative' stems from the observations that even though the Nd isotopic composition of
57 seawater is set by external inputs (e.g. Elderfield and Greaves, 1982; Goldstein et al., 1984),
58 changes in open ocean Nd isotopic compositions have been mainly attributed to water mass
59 mixing (e.g. Piepgras et al., 1979; Albarède and Goldstein, 1992). This assumption has been
60 substantiated by observed co-variations of Nd isotopes in deep waters in the western
61 Atlantic Ocean with salinity (von Blanckenburg, 1999) and silicate concentrations (Goldstein
62 and Hemming, 2003), but has been challenged by more recent observations.

63 For example, there is an increasing number of regions in the global ocean where a
64 straight forward correlation of seawater Nd isotopic compositions with predominant
65 hydrography is lacking (e.g. eastern Atlantic Ocean: Stichel et al. (2015); eastern and central

Equatorial Pacific Ocean: Grasse et al. (2012); Grenier et al. (2013); southeast Pacific Ocean: Jeandel et al. (2013); northern Indian Ocean: Singh et al. (2012); Amundsen Sea and eastern Pacific sector of the Southern Ocean, shelf area only: Carter et al. (2012); Weddell Sea and Atlantic sector of the Southern Ocean: Stichel et al. (2012a)). Furthermore, a growing number of studies has shown that Nd can be exchanged, released or adsorbed, on continental margins, a process called boundary exchange, which can significantly alter seawater Nd isotopic compositions (see summaries in Lacan and Jeandel (2005b) and Lacan et al. (2012)). Following surfaces of equal density (isopycnals), this non-conservative behaviour of Nd in the vicinity of continental margins can also leave a fingerprint in the open ocean, away from the area of actual seawater-sediment interaction (Lacan and Jeandel, 2001; Rickli et al., 2014).

An additional complication in understanding seawater Nd isotopic compositions as a potential water mass tracer is manifested by the observation that concentration profiles of dissolved Nd are mostly decoupled from profiles of Nd isotopes ("Nd paradox"; e.g. Goldstein and Hemming, 2003; Siddall et al., 2008). In detail, Nd concentration depth profiles resemble silicate profiles in the open ocean, showing depletions at the surface and enrichments with depth as well as an increase in bottom water concentrations along the conveyor belt (Elderfield and Greaves, 1982; de Baar et al., 1985; Elderfield et al., 1988; Bertram and Elderfield, 1993). This type of behaviour strongly suggests that processes other than inputs of Nd to the surface ocean and at ocean boundaries influence its vertical cycling. It has been suggested that reversible scavenging, a process of coupled adsorption and desorption between dissolved Nd in the water column and the marine particulate phase, may be important for the decoupling of concentrations and isotopes (Nozaki and Alibo, 2003a; Siddall et al., 2008; Arsouze et al., 2009; Oka et al., 2009; Rempfer et al., 2011).

However, most of the above cited studies tackle the problem using modelling tools as observational data from the ocean are still sparse.

Due to the time intensive nature and analytical involvement of the measurements, as well as the logistics of collecting large volume (5-10 L) seawater samples (e.g. van de Flierdt et al., 2012; Crocket et al., 2014), sample resolution for Nd isotopes in seawater will never be able to rival that of more conventional chemical and physical properties such as temperature, salinity, or density. However, the international GEOTRACES program represents an invaluable effort to significantly expand the observational database. Launched in 2010 with the guiding mission "to identify processes and quantify fluxes that control the distributions of key trace elements and isotopes in the ocean, and to establish the sensitivity of these distributions to changing environmental conditions" (Measures et al., 2007), the programme includes measurements of Nd concentrations and isotopic compositions of seawater as one of the key parameters to be analysed on every GEOTRACES section cruise (www.geotraces.org). Publications from the first sections during the 2007-2008 International Polar Year (Stichel et al., 2012a, 2012b) and the subsequent Atlantic program are just starting to become available (e.g. Stichel et al., 2015). Nevertheless, the number of Nd isotope observations has already increased from 880 individual measurements reported for the global ocean from the 1970's through 2011 (Lacan et al., 2012) to about twice this number in early 2015 (e.g. Carter et al., 2012; Stichel et al., 2012a, 2012b, 2015; Singh et al., 2012; Grasse et al., 2012; Jeandel et al., 2013; Grenier et al., 2013; Garcia-Solsona et al., 2014; Haley et al., 2014; Molina-Kescher et al., 2014; Huang et al., 2014; Rickli et al., 2014; Osborne et al., 2014; Basak et al., 2015).

We report the first results on dissolved Nd isotopic compositions and concentrations from GEOTRACES section GA02 along the flow path of North Atlantic Deep Water (NADW) in the

western Atlantic Ocean from Iceland in the north to the equator in the south (Rijkenberg et al., 2014). Twelve depth profiles of seawater Nd isotopic compositions and concentrations were analysed for 10 to 13 water depths each, almost doubling the available dataset in the subpolar North Atlantic, and tripling the number of data available in the subtropical Atlantic. Improved vertical sampling resolution as well as improved analytical precision allows us to reassess the Nd isotopic composition of NADW and the assumption that Nd isotopes behave conservatively away from continental inputs. Our new results confirm that water masses in the western North Atlantic can be depicted based on their Nd isotopic composition and provide water mass information in excess of what can be learned from classical hydrographic proxies or measurements of transient tracers such as CFCs (chlorofluorocarbons). Our new data furthermore highlight the non-uniform interplay between vertical processes and advection in different parts of the water column, making sample location and biogeochemical regimes a key variable when assessing and interpreting seawater Nd isotopic compositions.

2. Material and methods

2.1. Sampling

Twelve depth profiles of seawater samples were collected for Nd concentrations and isotopes on the RV *Pelagia* during the first two legs of the Dutch GEOTRACES cruise GA02 (64PE319 and 64PE321), that took place between the 28th of April and the 8th of July 2010 from Scrabster (Scotland) to Fortaleze (Brazil) via Bermuda (Fig. 1). Seawater samples for Nd isotope and concentration measurements were collected using either an ultraclean all-titanium frame CTD system (24 x 24 L), or a Niskin-type sampler mounted on a stainless steel rosette (24 x 25 L), and between 10 and 13 depths were sampled for Nd. Ten litre samples

were filtered on board the RV *Pelagia* using 0.2 µm Sartorius Sartoban 300 cartridges filters, which were rinsed with several litres of seawater prior to use. The samples were acidified on board to pH ~2 with subboiled distilled HCl (2 mL/L).

2.2. Analytical procedure

2.2.1. Sample preparation

Sample preparation, chemical separation and isotopic analyses were performed in the MAGIC Laboratories at Imperial College London (UK).

Between five and ten litres of seawater were weighted, spiked with ^{150}Nd (97.8% purity; provided by D. Vance, ETH Zürich) aiming for a spike ^{150}Nd : sample ^{150}Nd ratio of ~ 1 in order to minimise the error magnification on the ^{143}Nd/^{144}Nd ratio, and equilibrated for at least one week. The rare earth elements (REE) were pre-concentrated using C_{18} cartridges loaded with a complexing agent (65% bis(2-ethylhexyl) hydrogen phosphate and 35% 2-ethylhexyl dihydrogen phosphate) following the procedure of Shabani et al. (1992). In brief, after the pH of the samples had been raised to 3.5 using NH_4OH, they were pumped through a sequence of two cartridges (see Jeandel et al. (1998) for details) at a flow rate of 40 mL/min. Neodymium recovery was tested to be ~90% for pumping speeds at 20 and 40 mL/min, but dropped to ~80% when pumped at a faster speed of 60 mL/min. The cartridges were subsequently rinsed with 5 mL 0.01 M HCl in order to elute Ba, followed by 35 mL 6 M HCl (pumped at 10 mL/min) to collect the REE. All steps up to this point were performed in a Class 100 (ISO V) Laminar Flow hood within a general wet chemistry laboratory (i.e. pre-filtered air). Following elution, the samples were taken to a class 1000 (ISO VI) clean room laboratory, where all further steps were carried out in class 10 (ISO IV) laminar flow hoods. Samples were dried at 160 ˚C, and refluxed with 4 mL aqua regia (3 mL concentrated HCl + 1

160 mL concentrated HNO_3) at 120 ˚C for about 24 hours. The samples were subsequently
161 converted to nitric form by dissolving/drying three times in concentrated HNO_3.

162 *2.2.2. Column chemistry*

163 Neodymium was isolated using two stages of ion chromatography. In the first stage, REEs
164 were separated from any residual sample matrix using 100 µL Teflon columns, made from
165 shrink Teflon, with a reservoir of about 3 mL, about 2.3 cm in length and 3.0 mm inner
166 diameter filled with ~100 µL Eichrom TRU spec resin (100-150 µm bead size). After cleaning
167 the columns and the resin, the samples were loaded in 300 µL 1 M HNO_3. The matrix was
168 eluted in 1 mL 1 M HNO_3 and the REE were collected in 600 µL 4 M HCl. The REE fraction was
169 then dried at 120 ˚C. Yields of the TRU spec columns were measured to be about 95%.

170 The second stage of chemistry was performed to purify Nd from the other REE elements
171 using Savillex Teflon columns, with a reservoir of ~6 mL, 4 cm in length and 3.2 mm inner
172 diameter (resin bed volume: about 0.32 mL), filled with Eichrom Ln spec resin (20 – 50 µm
173 bead size). Due to the fine bead size of the resin, it is essential to use frit material of
174 sufficiently fine pore size. We used 1.5 mm thick Ultra-Fine polyethylene from SPC
175 Technologies (UK) with a maximum pore size of 25 µm and a mean pore size of 21 µm. The
176 samples were loaded and eluted with ~0.14 M HCl. Exact amounts of acid eluted varied
177 depending on the calibration used and details can be found in Crocket et al. (2014).

178 The TRU spec resin is known to leak organics (Gault-Ringold and Stirling, 2012), and such
179 organics can compromise the yields of a secondary column as indicated by yield tests on our
180 Ln columns that initially showed Nd recoveries that varied between 2 and 80%. In order to
181 resolve this problem an oxidation step with perchloric acid (250 µL concentrated $HClO_4$ + 1
182 mL concentrated HNO_3) was added in between the two columns, leading to consistently

higher column yields (>60%) for the Ln column (note that ~40% Nd loss on this column is deliberately introduced during calibration in order to keep Pr levels low).

2.2.3. Measurements

The Nd isotopic ratio is expressed as ε_{Nd} that denotes the deviation of a measured $^{143}Nd/^{144}Nd$ ratio from the Chondritic Uniform Reservoir (CHUR = 0.512638, (Jacobsen and Wasserburg, 1980)) in parts per 10 000 as per the following equation:

$$\varepsilon_{Nd} = \left[\frac{(^{143}Nd/^{144}Nd)_{sample}}{(^{143}Nd/^{144}Nd)_{CHUR}} - 1\right] \times 10\,000 \quad \text{(Equation 1)}$$

Neodymium isotopic compositions and concentrations were measured as Nd oxides (NdO^+) over a 19 month period on a Thermo Finnigan Triton thermal ionization mass spectrometer (TIMS) equipped with a pyrometer. Details on the measurement protocol can be found in Crocket et al. (2014).

Accuracy was achieved by correcting sample $^{143}Nd/^{144}Nd$ results for the offset of five filaments of 5 ng or 15 ng JNdi-1 standard per turret (typical batch of samples: 16) to the JNdi-1 reference value of 0.512115 (Tanaka et al., 2000) and monitored using 10 ng or 15 ng loads of column processed rock standard BCR-2 (external reproducibility for the BCR-2 rock standards was 20 ppm on $^{143}Nd/^{144}Nd$; ε_{Nd} = 0.01 ± 0.20, 2sd, n = 12). The long term average $^{143}Nd/^{144}Nd$ ratio for 5 to 15 ng JNdi-1 loads on the MAGIC Triton TIMS during the 19 months duration of seawater analysis was 0.512103 ± 0.000011 (ε_{Nd} = -10.44 ± 0.22, 2sd, n = 70). To determine the true external reproducibility for seawater samples, two large homogeneous water samples from the Bermuda Atlantic Time Series Station BATS (15 m and 2000 m depth) were used as in-house seawater standard (van de Flierdt et al. 2012). Results are reported in Table 1 and are in an excellent agreement with the results from the international

GEOTRACES intercalibration exercise obtained by 13 different laboratories (van de Flierdt et al., 2012). It is worth noting that the samples were purified and analysed over a period of 19 months, between 3 and 5 years after initial sample collection. Hence, the present results show that filtered and acidified seawater can be stored in pre-cleaned containers for up to five years without compromising the isotopic composition or concentration of Nd. Typical procedural blanks (chemistry and mass spectrometry) were 0.8 to 11.2 pg, which translates to less than 0.2% of the Nd content of the most depleted sample analysed. Therefore no blank correction was applied.

3. Results

3.1. Overview of seawater Nd isotopic compositions and concentrations

The track for the Dutch GA02 section cruise followed the deepest part of the Northwest Atlantic Ocean and the flow path of NADW (Figs. 1 and 2), starting from the Irminger Sea (station 2: 64.00˚ N, 34.25˚W) down to the south of the Sargasso Sea (station 30: 18.57˚ N, 57.61˚W) (Table 2) and further into the Southwest Atlantic to the Falkland Islands (third leg – see http://www.geotraces.org/, Rijkenberg et al. (2014) and Middag et al. (2015) for details on the entire cruise track; not part of this study).

In order to directly compare seawater Nd isotopic compositions and concentrations with water mass hydrography, Table 2 identifies water masses encountered at the twelve stations based on physical properties and nutrient concentrations (Rijkenberg et al., 2014; Mawji et al., 2015). Water mass boundaries (Table 2; see also isopycnals in Figures 2a and c) are based on the potential density anomaly (σ_θ) following Rhein et al. (2011) and were found to be in good agreement with other observed properties along the GA02 section (e.g. salinity,

temperature, oxygen and nutrient concentrations). We are aware that the density ranges chosen are sometimes broad and can therefore overestimate the depth range of certain water masses. However, the intention was to assign water masses to every sample analysed in the present study. The hydrography description as well as the water mass boundaries were determined on the 24 depths sampled for each station, whereas only a maximum of 13 depth were collected for Nd analyses and are therefore reported in Table 2. Hence, the hydrographic values in Table 2 may not always reflect the full hydrographic characteristics used to define the water masses (e.g. the maximum or minimum value may be missing in the table). The exhaustive dataset for hydrography and nutrients can be found in the GEOTRACES Intermediate Data Product (Mawji et al., 2015) as well as in Rijkenberg et al. (2014).

Table 3 lists abbreviations for water masses and currents used in the text. Figure 3 provides Θ-S plots for individual stations from the GA02 section and Figure 4 shows results for Nd isotopic compositions and concentrations of seawater profiles grouped in three different geographic regions: the Irminger Sea, the SE Labrador Sea & Grand Banks, and the Sargasso Sea. This grouping was chosen to reflect that water masses change their characteristics from the subpolar gyre (Irminger Sea: stations 2,5,6; Fig. 1) to the subtropical gyre (Sargasso Sea: stations 15,19,21,25,28,30; Fig. 1), with the SE Labrador Sea / Grand Banks region marking a transitional area, with characteristics that deserve separate consideration (stations 9,11,13).

The Nd isotopic composition for the entire study area is presented in Figure 2a in a section view contoured by isopycnals separating the various water masses (see Table 2). Seawater ε_{Nd} in the North Atlantic ranges from -17.0 in the surface waters of the southeastern Labrador Sea to -9.4 in the subsurface waters of the subtropical gyre. In detail,

three more radiogenic areas (i.e. relatively high ε_{Nd} values) can be identified: (i) the bottom waters at latitudes > 50°N ($\varepsilon_{Nd} \approx -11$), (ii) the bottom waters at the southernmost stations (e.g. stations 25 to 30; $\varepsilon_{Nd} \approx -11.5$); and (iii) the surface waters of the subtropical North Atlantic ($\varepsilon_{Nd} \approx -10.5$; Equatorial Surface Water (ESW) and Western North Atlantic Central Water (WNACW)). In contrast, the surface waters of the subpolar North Atlantic are characterised by less radiogenic Nd isotope ratios ($\varepsilon_{Nd} \approx -17$). Although being diluted, this tongue of less radiogenic Nd isotopic composition extends northwards as well as southwards to 35°N.

Neodymium concentrations are presented in a section view in Figure 2b, contoured by apparent oxygen utilisation isoline (AOU [µmol/kg], a measure for decomposition of organic matter). The apparent oxygen utilisation is the difference between the measured oxygen concentration and the oxygen saturation concentration at the given pressure/depth, temperature and salinity; in other words, high values for AOU mean that more oxygen has been consumed and more organic matter has been decomposed. Overall most of the section is dominated by Nd concentrations in the range of 17 to 20 pmol/kg. In detail, the northernmost profiles (e.g. north of 40˚N) show relatively small gradients in Nd concentrations from top to bottom, with the lowest concentrations being found in the deep and bottom waters in the Irminger Basin (stations 2 to 6, [Nd] ≈ 16 pmol/kg) and the highest values in the surface and subsurface of the Labrador Sea (station 9; [Nd] ≈ 21 pmol/kg) (Figs. 1 and 2b). Stronger gradients in Nd concentrations and a first order increase of values from top to bottom can be found in all stations of the western subtropical North Atlantic (stations 15 to 30; [Nd] ≈ 13 pmol/kg in surface waters, [Nd] ≈ 32 pmol/kg in bottom waters). This increase, however, is not linear as constant Nd concentrations can be found at intermediate to deep levels in the water column (1000-2500 m) (Fig. 2b).

For comparison with the Nd sections, Figure 2c presents a section with salinity results from all samples collected during the northern part of the GA02 cruises. This section shows similarities with the Nd isotopic compositions (Fig. 2a): the unradiogenic surface water of the subpolar gyre are characterised by lower salinity, and the radiogenic surface water of the subtropical gyre by high salinity. Both Antarctic Intermediate and Antarctic Bottom Water can be recognised on the salinity section by tongues of lower salinity waters.

3.2. Detailed comparison of Nd isotopic composition, Nd concentration, and hydrography of encountered water masses

3.2.1. Surface and upper-layer water masses

The most prominent current in the subpolar North Atlantic is the North Atlantic Current (NAC, Fig. 5), the northeastward extension of the Gulf Stream, which brings warm and salty water of subtropical origin into the subpolar North Atlantic. Along its journey in the subpolar North Atlantic, the NAC splits and mixes with other surface currents forming the anti-clockwise flowing North Atlantic Subpolar Gyre (Schmitz, 1996). The subsurface layer (between 200 and 1000 m) of the subpolar gyre is composed of Subpolar Mode Water (SPMW), which is formed by mixing of subtropical and polar water masses followed by winter time convection, and is the precursor of Labrador Sea Water (McCartney and Talley, 1982; Hanawa and Talley, 2001). In the subpolar area of the present study, (sub)surface waters are defined as the waters overlying Upper Labrador Sea Water (ULSW; e.g. $\sigma(\theta) <$ 27.68 kg/m^3). The depth range they occupy can vary from 150 m at stations 5 and 6 in the Irminger Sea to 750 m at station 13, around the Grand Banks (Table 2). Neodymium isotopic compositions in surface waters range from -15.2 to -13.4 in the Irminger Sea, and -17.0 to -15.0 in the SE Labrador Sea, to -16.9 to -11.5 around the Grand Banks. For the same

samples, Nd concentrations show a range from 16.5 to 21.8 pmol/kg. While regional differences are clearly resolvable, the combination of our new surface seawater measurements with previously published results (Fig. 5) highlights the generally well mixed signature of surface waters within the subpolar gyre (Fig. 5) and their unradiogenic character ($\varepsilon_{Nd} \approx -15$). Subsurface variations are relatively minor in the Irminger Sea but significant around the Grand Banks (Fig. 4c,d) where the topmost sample is very unradiogenic ($\varepsilon_{Nd} \approx -14$ at station 11 to $\varepsilon_{Nd} \approx -17$ at stations 9 and 13) followed by a pronounced shift towards more radiogenic values in the subsurface waters ($\varepsilon_{Nd} \approx -15$ at station 9 to $\varepsilon_{Nd} \approx -12$ at stations 11 and 13). The Nd concentrations are higher (between 17.7 and 21.1 pmol/kg) and the salinity lower at the surface around the Grand Banks and the subsurface waters are less concentrated in Nd, coinciding with a sharp increase in salinity (Table 2).

In contrast to the subpolar gyre, the subtropical gyre circulates clockwise, and occupies the latitudes from ~10˚N to ~40˚N in the North Atlantic basin (Fig. 5). Its most prominent current is the Gulf Stream (GS), which forms the western and northern part of the gyre. Below the surface layer, North Atlantic Central Water (NACW) occupies the Atlantic thermocline and is characterized by a nearly straight θ-S relationship between 15 and 35°N (Fig. 3; Tomczak, 2001). Subtropical Mode Water (STMW) is part of NACW and is a vertically homogenous water mass (Worthington, 1959; Hanawa and Talley, 2001). Equatorial Surface Water (ESW) constitutes the surface return flow of NACW, but is a distinct water type due to evaporation/precipitation-driven transformation upon upwelling near the equator. In contrast to STMW, which is characterised by a well-defined Nd isotopic composition ($\varepsilon_{Nd} = -9.6 \pm 0.2$) and Nd concentration (14.1 ± 1.2 pmol/kg; 2sd, n = 6, Table 2), Western NACW features large variability in its Nd characteristics in the northern subtropical gyre, with ε_{Nd} values ranging from -13.5 to -9.4 and Nd concentrations from 12.1 to 18.1 pmol/kg (stations

15, 19 and 21). In the southern part of the subtropical gyre, the Nd features of Western NACW are more constrained (ε_{Nd} = -11.0 to -9.9 and [Nd] = 14.5 to 18.1 pmol/kg; station 25, 28 and 30). Equatorial Surface Water is found at stations 19 to 30 (Fig. 1) and shows a very homogenous signature in the northern part of the gyre (stations 19 and 21; ε_{Nd} = -9.8 to -9.5 and [Nd] $\approx$ 13.3 pmol/kg; 9 to 50 m depth; Table 2; Fig. 4f). In the southern subtropical gyre (stations 25 to 30), the Nd isotope ratios are less radiogenic than in the northern gyre, and the Nd concentrations are higher (ε_{Nd} ≈ -10.3; [Nd] = 16.7 pmol/kg; 11 to 152 m depth; Table 2; Figs. 4 e,f). Surface samples are less saline than in the northern part of the gyre (Fig. 3b), suggesting external freshwater influence (see section 4.2.2).

3.2.2. North Atlantic Deep Water (NADW) and its constituents

In the subtropical western Atlantic Ocean, NADW is subdivided into three main layers: upper-, middle-, and lower-NADW (Schmitz, 1996). These three components refer to the source water masses which constitute NADW and are formed in the subpolar region. The name NADW is used for intermediate to deep waters once they leave the mixing area of the subpolar gyre and are advected south in the deep western boundary current.

3.2.2.1. Upper-NADW (ULSW and LSW)

The least dense components of NADW in the northern North Atlantic are the two classes of Labrador Sea Water: Upper-LSW (ULSW) and Classical-LSW (which will be called LSW hereafter). Upper Labrador Sea Water is formed every winter by convection in newly generated eddies in the southern, central and northern Labrador Sea (Smethie et al., 2000; Stramma et al., 2004; Kieke et al., 2006). ULSW is less dense than LSW and shows higher CFC concentrations indicating that it was ventilated more recently (Swift, 1984; Stramma and Siedler, 1988; Smethie et al., 2000; Steinfeldt and Rhein, 2004; Kieke et al., 2006). In the

GA02 section, ULSW is the least dense component of NADW and is identified by potential density ranges of $27.68 < \sigma_\theta < 27.74$ kg/m^3. Its Nd characteristics are well constrained within the subpolar gyre, with $\varepsilon_{Nd} = -14.3 \pm 0.3$ and [Nd] = 18.3 ± 0.7 pmol/kg (n = 10, 2sd).

Labrador Sea Water is formed by deep convection due to surface water cooling during winter time in the central Labrador Sea (Talley and McCartney, 1982; Sy et al., 1997; Yashayaev and Loder, 2009). It is characterised by low salinity, high oxygen content and high anthropogenic CFC concentrations, and potential density ranges of $27.74 < \sigma_\theta < 27.81$ kg/m^3 in the present study. It can be distinguished from ULSW by an O_2 maximum (Talley and McCartney, 1982; Swift, 1984; Sy et al., 1997; Smethie et al., 2000; Steinfeldt and Rhein, 2004; Kieke et al., 2006). The Nd isotopic composition of LSW is -13.7 ± 0.9 (2sd, n = 8, Figs. 2a and 4b,d), with the spread in data being mainly due to mixing with less radiogenic North East Atlantic Deep Water (NEADW) in the SE Labrador Sea and off the Grand Banks (see Table 2). Neodymium concentrations within LSW are relatively homogenous with 17.5 ± 0.9 pmol/kg (2sd, n = 8, Figs. 4 a and c). These results are in good agreement with the study of Lacan and Jeandel (2005a) where LSW was characterised by $\varepsilon_{Nd} = -13.8 \pm 1.0$ and [Nd] = 19.7 ± 6.97 pmol/kg in the subpolar gyre (n = 5, 2sd).

Both ULSW and LSW spread at mid-depth in three principal directions in the North Atlantic Ocean: northeastward into the Irminger Basin, southeastward across the Mid Atlantic Ridge, and south within the deep western boundary current (Lavender et al., 2000; Kieke et al., 2006; Kieke et al., 2009; Rhein et al., 2011) (Fig. 1). At latitudes south of 35˚N, Mediterranean Outflow Water (MOW), characterised by high salinity and high potential temperature, mixes with both ULSW and LSW to form 4 Sv (1 Sv = 10^6 m^3/s) of the water mass called upper-NADW (Schmitz, 1996). Leaving the subpolar gyre, station 15 south of the Grand Banks did not provide any samples in the density range of ULSW. This water mass

was, however, identified in 1250m water depth at stations 19 to 30, just below the well-defined silicate maximum corresponding to Antarctic Intermediate Water (AAIW). It is the presence of and mixing with AAIW, characterised by radiogenic Nd values in the South Atlantic (e.g. $\varepsilon_{Nd} \approx -8.7$, see Jeandel, 1993), which most likely explains why the ε_{Nd} values of USLW become progressively more radiogenic when flowing southward, from -13.8 at station 19 to -12.2 at station 30 (Figs. 2a and 4f). Neodymium concentrations within subtropical ULSW are very similar to those encountered in the subpolar gyre (~17.5 pmol/kg, Fig. 4e). Labrador Sea Water occupied depths between 1500 and 2000m in the subtropics during expedition GA02 (stations 15 to 30) and is associated with a small, but resolvable oxygen maximum, ε_{Nd} of -13.3 ± 0.3 (2sd, n = 6), and comparable Nd concentration to the subpolar area (~17.5 pmol/kg, Fig. 4e).

Overall, the ε_{Nd} signature of upper-NADW (encompassing ULSW and LSW) in the subtropical North Atlantic is -13.2 ± 1.0 and the Nd concentration is 17.6 ± 1.1 pmol/kg (2sd, n = 10).

3.2.2.2. Middle-NADW (NEADW)

Middle-NADW is called North East Atlantic Deep Water (NEADW) in the northern North Atlantic, and it is a mixture of 2 Sv Iceland Scotland Overflow Waters (ISOW), 2 Sv Lower Deep Water (LDW; this is modified Antarctic Bottom Water, after its northward flow through the Atlantic Ocean), and 2 Sv of a mixture of Atlantic Water (AW) and LSW (Schmitz, 1996). The characteristics of NEADW are a salinity maximum (due to the Atlantic Water coming from the Subtropical Atlantic), an oxygen minimum (due to the LDW), a CFC concentration lower than LSW and Denmark Strait Overflow Water (DSOW; see next section) and an intermediate potential density between LSW and North West Atlantic Bottom Water

392 (NWABW) (Swift, 1984; Dickson and Brown, 1994; Smethie et al., 2000; Stramma et al.,
393 2004). In the present study, it occupies a potential density range of $27.81 < \sigma_\theta < 27.88$ kg/m^3.
394 In the Irminger Basin, it is detected at 1900 m (station 2) and between 2000 and 2750 m
395 (stations 5 and 6; Fig. 1, Table 2), at deeper levels of 2250 and 2550 m in the SE Labrador
396 Sea, and at 2500 and 3500 m to the east of the Grand Banks. The typical salinity maximum of
397 NEADW could be detected at $\sigma_\theta \approx 27.85$ to 27.86 kg/m^3 (Fig. 3c) and its Nd isotopic
398 composition was determined to be ε_{Nd} = -12.9 to -12.1, with Nd concentrations in the range
399 of 15.9 to 17.9 pmol/kg (stations 2,4,5,9,11,13; n = 8; Figs. 1 and 3, Table 2).

400 In the Subtropical area (stations 15 to 30, Fig. 1, Table 2), middle-NADW flows between
401 2000 and 3000 m depth and is characterised by a small O_2 minimum. It is slightly saltier than
402 in the subpolar area (S = 34.96 ± 0.02; 1sd), and has a potential temperature of 2.99 ± 0.35˚C
403 (1sd). The ε_{Nd} value is -12.3 ± 0.4 and its Nd concentration is 18.0 ± 1.1 pmol/kg (2sd, n = 6).

404 Overall, NEADW shows a rather constant Nd isotopic composition throughout the study
405 area (ε_{Nd} = -12.4 ± 0.5, 2sd, n = 14; all stations in subpolar and subtropical areas). The most
406 likely explanation for this observation is that none of our stations are situated close to the
407 actual source areas of an important component of NEADW, Iceland-Scotland Overflow
408 Water (ISOW; ε_{Nd} = -8.2 ± 0.6; Lacan and Jeandel, 2004b). Hence, we are sampling a mixed
409 signature, which is also supported by the relatively weak salinity maximum of this water
410 mass (Fig. 3c).

411 *3.2.2.3. Lower-NADW (NWABW)*

412 Lower-NADW originates in the northern North Atlantic as North West Atlantic Bottom
413 Water. Its main contributor is Denmark Strait Overflow Water (DSOW), a dense water mass
414 that overflows the Denmark Strait (sill depth of ~600 m, Fig. 1). This water mass is the

densest component of NADW with σ_θ > 27.88 kg/m^3 (Fig. 3c). It is characterized by a salinity minimum, an oxygen maximum, and high CFC concentration (Swift, 1984; Dickson and Brown, 1994; Smethie et al., 2000; Stramma et al., 2004). In the subpolar Atlantic, NWABW is comprised of 3 Sv DSOW, 3 Sv in total of entrained LSW and SPMW, and 1 Sv western LDW joins at about 50˚N. Further south, in the Subtropical Atlantic at about 30°N, an additional 1 Sv of western LDW is admixed to NWABW around 30˚N, forming 8 Sv lower-NADW (Schmitz, 1996).

Regarding the Nd characteristics of NWABW, we observe less of an evolution with latitude, but rather a drastic change for NWABW from its values close to the source region (e.g. stations 2 to 6, ε_{Nd} = -11.7 to -10.6, n = 6, Table 2; for comparison, DSOW has a Nd isotope signature of ε_{Nd} = -8.4 ± 1.4; Lacan and Jeandel, 2004a) to values outside the Irminger Sea (ε_{Nd} = -12.4 ± 0.5, 2sd, n = 18). Indeed, NWABW displays a change of ε_{Nd} ≈ 1.1 for a flow path of ~650 km from station 2 to 6 in the Irminger Basin (Fig. 1) whereas only a change of ~0.9 ε_{Nd} occurs over ~5500 km from station 9 to 30. This observation is in agreement with relatively constant salinity values for NWABW throughout the subtropical North Atlantic (Fig. 2c) and indicates that efficient mixing with overlying and less radiogenic water masses already happens in the subpolar gyre prior to export as part of lower-NADW.

Since the average ε_{Nd} value for lower-NADW is within error identical to the ε_{Nd} value of middle NADW (ε_{Nd} = -12.3 ± 0.4, 2sd, n = 6), we will combine both in the following under the name lower-NADW. This water mass is characterised by an integrated ε_{Nd} value of -12.4 ± 0.4 and a Nd concentration of 22.5 ± 8.2 pmol/kg (2sd, n = 16).

3.2.3. *Southern Ocean water masses: AAIW and AABW*

Antarctic Intermediate Water (AAIW) and Antarctic Bottom Water (AABW) are both formed in the Southern Ocean and exported northward in all ocean basins. Due to its recent ventilation, AAIW is characterised by a relative maximum in dissolved oxygen content. In the Atlantic Ocean, it can be depicted as a tongue of low salinity and high nutrient (phosphate, nitrate and silicate) water spreading northwards at about 1000 m depth up to ~25-30˚N (Rijkenberg et al., 2014; Middag et al., 2015). Due to these characteristics, it can be recognised at stations 25 to 30 of the present study (Fig. 1). Only three samples were collected for Nd in this water mass, yielding ε_{Nd} values of -11.2 ± 0.3 and a Nd concentration of 17.8 ± 1.2 pmol/kg (2sd, n = 3, Tables 2). This result is less radiogenic than the value of -10.1 reported for modified AAIW at 8°N (Huang et al., 2014).

Northward advection of AABW into the Atlantic Ocean (up to 45˚N) can typically be recognised by relative high nutrient concentration and by low salinity (Tomczak, 2001; Rijkenberg et al., 2014). These properties are encountered in the entire subtropical area of the present study at depths below ~4500 m. The ε_{Nd} value of -12.2 ± 1.0 is significantly less radiogenic than that of AABW in the South Atlantic (ε_{Nd} = -8.5 ± 0.3; Jeandel (1993)), and becomes progressively less radiogenic towards the north. The Nd concentration of modified AABW is 31.9 ± 3.4 pmol/kg (2sd, n = 9, Table 2).

4. Discussion

4.1. Reassessment of the neodymium isotope signature of seawater - a water mass proxy?

North Atlantic Deep Water, once exported from the subpolar gyre, can be separated into upper- and lower-NADW with distinct Nd isotopic compositions: ε_{Nd} = -13.2 ± 1.0 (2sd, n = 10) and ε_{Nd} = -12.4 ± 0.4 (2sd, n = 16) respectively (Fig. 4f). While these values overlap within uncertainty, an unpaired t-test shows that the results differ at the 95% confidence level. This observation matters, as our new results for upper-NADW show excellent agreement with the traditionally cited NADW value of -13.5 ± 0.5 (Piepgras and Wasserburg, 1987; Lacan and Jeandel, 2005a). The new (and better resolved) data for lower-NADW in the subtropical area are, however, more radiogenic. This distinction should be kept in mind when making palaeoceanographic interpretations (e.g. Roberts et al., 2010; Wilson et al., 2014).

Our new data provides a unique opportunity to reassess the viability of seawater Nd isotopic compositions as a 'quasi-conservative water mass tracer' in the western North Atlantic. To test this hypothesis, and to follow up and expand on the initial work by Goldstein and Hemming (2003), we will compare our data to (i) salinity, (ii) SiO_2, (iii) neutral density (Υ^n), and (iv) CFC data available from the same cruises (Rijkenberg et al., 2014).

4.1.1. Neodymium isotopes vs salinity

Conservative behaviour of Nd isotopes in Atlantic seawater has been suggested for deep waters below 2500 m by correlation with salinity (see Figs. 9 and 10 in Goldstein and Hemming (2003)). Figure 6a shows an updated version of this figure, including our new deep water data (>2500 m) as well as results for water masses as shallow as ULSW from all stations in the present study and previously published data (>1000 m in the subtropical gyre,

and shallower in the subpolar gyre). In order to construct the mixing envelop, the following equation is used (Mariotti et al., 1988):

$$\varepsilon Nd_{Mix} = \frac{(\varepsilon Nd_{SW1} \cdot [Nd]_{SW1} \cdot f_{SW1}) + (\varepsilon Nd_{SW2} \cdot [Nd]_{SW2} \cdot f_{SW2})}{f_{SW1} \cdot [Nd]_{SW1} + f_{SW2} \cdot [Nd]_{SW2}} \quad \text{(Equation 2)}$$

The parameter 'f' denotes the respective mass fractions (f_{SW1} + f_{SW2} = 1). SW1 and SW2 refer to a northern and a southern end-member respectively, whereas the subscript 'Mix' refers to a mixture of the two endmembers. Southern Ocean water (ε_{Nd} ≈ -8.5; S = 34.65) and North Atlantic Deep Water (ε_{Nd} ≈ -13.5; S = 34.95) are taken as endmembers (Goldstein and Hemming, 2003) and encapsulate most of the previously published deep waters (i.e. >2500m; Goldstein and Hemming, 2003) and all of our new data points from below 2500m water depth. The utilisation of a 'North Atlantic Deep Water endmember' is however problematic, and in fact misleading, when extending the compilation to the subpolar gyre and to shallower source waters contributing to NADW. For example, data for ULSW from this study plot outside the mixing envelop, as these waters are (i) fresher in the subpolar area and (ii) saltier in the subtropical region for a given Nd isotopic composition. Another way to describe these data is to state that the Nd isotopic composition of ULSW in the subpolar gyre can be significantly less radiogenic than the traditionally chosen NADW endmember. In the subtropical gyre, in contrast, mixing with AAIW quickly changes the properties of ULSW.

4.1.2. Neodymium isotopes vs silicate concentrations

It is furthermore interesting to plot seawater Nd isotopic compositions versus silicate concentrations for samples below and above 2500m (Fig. 6b). Since silicate is a macro-nutrient, its concentration in the upper part of the water column is governed by biological uptake. Concentrations in deeper waters are a function of remineralised silicate, and show an increase along the global conveyor belt with increasing age of water masses. Following

Goldstein and Hemming (2003), two simple endmembers are assumed for the Atlantic Ocean: one that shows high nutrient (and hence silicate) concentrations and relatively radiogenic Nd isotopic compositions and is sourced in the south (AABW; $\varepsilon_{Nd} \approx -8.5$ and $[SiO_2] \approx 125$ µmol/kg) and a second with lower nutrient concentrations and lower ε_{Nd} values, which reflects NADW exported from the subpolar gyre ($\varepsilon_{Nd} \approx -13.5$ and $[SiO_2] \approx 12$ µmol/kg; Goldstein and Hemming, 2003). While such a simplistic mixing relationship encloses most of the published seawater data, our new results from NWABW in the subpolar region clearly plot outside the mixing envelope (Figure 6b) (Table 2). This may be partially due to boundary exchanges with the nearby margin. It however primarily reflects that the source water for NWABW is significantly more radiogenic than readily mixed NADW (i.e. DSOW = -8.4 ± 1.2, (Lacan and Jeandel, 2005a)). The samples from shallower water masses (e.g. ULSW and LSW), in contrast, do fit in the mixing envelope in both the subpolar and subtropical gyres. Similarly to NWABW, they however reveal a striking trend towards the source composition of (U)LSW, which is the least radiogenic water mass in the North Atlantic. Due to similar silicate concentrations in NW and NE Atlantic source waters contributing to NADW, Nd isotopes are uniquely suited to unravel the provenance of the source water mass. Figure 6b also highlights that the different source signatures are largely mixed away by the time deep waters leave the subpolar region. It is worth noting that this delicate balance may have been different in the past, when advection strength and/or density structure in the North Atlantic were different.

4.1.3. Neodymium isotopes vs neutral density

A more appropriate way to assess the level of 'conservativeness' of Nd isotopes, is to illustrate Nd isotope results versus neutral density. This approach links shallow and deep

source waters in the subpolar NW and NE Atlantic with exported NADW in the subtropical area, and is presented in Figure 7. The depth range illustrated is the one featuring Υ^n > 27.8 kg/m^3, corresponding to the water mass of ULSW and those with higher densities. Overall, there exists a strong relationship between the Nd isotopic compositions of intermediate to deep water in the North Atlantic and neutral density, highlighting that the seawater Nd isotope signature is well constrained for a given neutral density, and therefore for a given intermediate or deep water mass. There are, however, some interesting deviations from this trend, which will be discussed below.

In the subpolar region, the samples collected from the NWABW layer at stations 11 and 13 are offset from the general negative correlation to more radiogenic Nd isotopic compositions (Figs. 1 and 7c, orange squares). When considering Nd concentrations of all samples vs neutral density (Fig. 7b), there is not much variation in [Nd] with increasing densities for 27.8 kg/m^3 < Υ^n < 28.1 kg/m^3 (e.g. ULSW, LSW and NEADW). However, once the density level of NWABW is encountered, a pronounced increase in Nd concentration for a given density can be observed (stations 11 and 13 off the Grand Banks; Figs. 7b and 7d). Surface sediments collected in the southeastern Labrador Sea feature ε_{Nd} = -20.1 ± 0.1 and a Nd concentration of 29.23 ppm (Innocent et al., 1997), whereas turbidites sampled in the Newfoundland Basin show ε_{Nd} = -24.5 ± 0.4 and Nd concentration of 22.1 ppm (McLennan et al., 1990). Therefore, sediment remobilization could explain the shift towards less radiogenic Nd isotope composition and higher Nd concentrations observed for the samples collected in the NWABW layer at stations 11 and 13. Indeed, sediment remobilisation associated with the nepheloid layer has been shown to be a source of aluminium around the Grand Banks (Middag et al., 2015). The slight decrease in Nd concentrations with increasing density

546 observed for the other samples from the subpolar region may hint towards Nd adsorption
547 onto suspended particles.

548 In the subtropical region, the samples from the ULSW layer (stations 25 and 30) feature a
549 Nd isotopic composition too radiogenic (ε_{Nd} = -12.6 ± 0.3 and ε_{Nd} = -12.2 ± 0.3 respectively,
550 Table 2) compared to the samples taken in the same water mass at stations 19 and 21 (ε_{Nd} =
551 -13.8 ± 0.3 for both samples, Table 2, Figs. 1 and 7a, blue diamonds). The Nd concentration
552 of ULSW is, however, homogeneous with [Nd] = 17.7 ± 1.3 pmol/kg (2sd, n = 4, Fig. 7b). This
553 shift towards more radiogenic ε_{Nd} values for stations 25 and 30 most likely reflects mixing
554 between ULSW and AAIW as indicated in section 3.2.2.1, with the most radiogenic values
555 being observed in the southernmost station 30. Interestingly, the trend of slightly higher Nd
556 concentrations for a given density range described for NWABW samples from stations 11
557 and 13 is even more pronounced for lower-NADW and modified AABW samples in the
558 subtropical gyre (stations 15 to 30), with deviations from the rather constant Nd
559 concentrations of up to 15 pmol/kg following a distinct trend. Neodymium isotopic
560 compositions for all of these samples, however, seem to only show a small deviation from
561 the overall negative correlation between Nd isotopic composition and neutral density (Fig.
562 7a), requiring a mechanism to decouple Nd isotopic compositions and concentrations in
563 deep samples from the subtropical gyre. We will return to this point in section 4.3.

564 *4.1.4. Neodymium isotopes and CFC concentrations*

565 Chlorofluorocarbons are anthropogenic substances that have entered the atmosphere
566 since the 1930s, but were phased out due to their harmful effect on the ozone layer
567 following the Montreal Protocol. Hence, decreasing atmospheric CFC concentrations have
568 been observed since the 1990s (Smethie et al., 2000). In the mixed layer, CFCs are typically in

569 equilibrium with the atmosphere. Therefore, their concentration in the mixed layer equals
570 the concentration at saturation, which in turn depends on temperature (i.e. solubility is
571 higher in colder water) (e.g. Rhein et al., 2015). CFCs are chemically stable in seawater and
572 are thus excellent tracers of recently ventilated components of NADW (e.g. Smethie et al.,
573 2000). Figure 8 shows results of CFC measurements from the northern part of the
574 GEOTRACES section cruise GA02 in comparison to the Nd isotopic composition of waters.
575 The dominant features are high CFC-11 contents in ULSW, LSW and NWABW (i.e. DSOW) in
576 the subpolar region, as previously summarised by Smethie et al. (2000), Stramma et al.
577 (2004) and Rhein et al. (2015). Overall, Nd isotopic compositions follow CFC distributions
578 quite closely in the subpolar region, but are less tightly coupled in the subtropical areas
579 south of 40°N, as is to be expected based on the observation that CFC concentrations fall
580 below 1 pmol/kg in intermediate and deep waters and are not suitable for tracking modified
581 AAIW and AABW in the subtropical Atlantic (e.g. Orsi et al., 1999; Orsi et al., 2002).

582 This first direct and regional comparison of seawater Nd isotopic composition and CFC
583 contents reveals some important insights into the complementary strength of both tracers.
584 Firstly, the two recently ventilated water masses delineated by the CFC data (ULSW/LSW and
585 DSOW) show similar CFC-11 levels (3.5 pmol/kg for ULSW/LSW at station 9 and 4.3 pmol/kg
586 for DSOW at station 2), whilst they are characterised by very different ε_{Nd} values (-14.3 for
587 ULSW/LSW at station 9 and -11.5 for DSOW at station 2). This observation stresses that the
588 Nd isotopic composition of seawater is a tracer for water mass provenance and is set by the
589 inputs of Nd to the ocean from the continents (e.g. radiogenic Nd isotopic composition
590 around young volcanic islands versus unradiogenic Nd isotopic composition around old
591 continental crust). In regions with proximal continental inputs and active convection, this

leads to a coupling of CFC and Nd isotope data, with Nd isotopes adding a provenance dimension to recently ventilated water masses.

Secondly, we would like to draw attention to the detailed relationship of CFCs and Nd isotopes in the region around 50° and 65°N. The maximum in CFC concentrations in surface waters (~4.4 pmol/kg) is located around ~60°N where temperatures are cold ($\theta \approx 5.6$ °C at surface of stations 5 and 6, Table 2), promoting uptake of CFCs. The lowest surface water Nd isotopic compositions ($\varepsilon_{Nd} \approx -16.9$) are, however, encountered around 52°N, coupled with higher temperatures ($\theta \approx 9.2$ °C at station 9), slightly lower salinity and higher Nd concentrations ([Nd] = 21.3 pmol/kg). This reflects the influence of the Labrador Current, itself affected by riverine inputs from the old continental source regions around Newfoundland (see also section 4.2.1). In today's ocean, the most unradiogenic component of NADW, which is ULSW ($\varepsilon_{Nd} = -14.3$), does not directly reflect the most unradiogenic inputs into the area from the Labrador Coast ($\varepsilon_{Nd} \approx -25$; see Fig. 5). This observation may become important for explaining the less radiogenic Nd isotopic composition of northern sourced water masses observed in studies of seawater during the last glacial cycle (Böhm et al., 2015). Here, ε_{Nd} values as low as -18 at peak Dansgaard-Oescher events (Greenland warm periods) are difficult to explain with waters sourced from the Labrador Sea. Instead, they require involvement of a more unradiogenic source, such as identified here around the Grand Banks (or previously described for Baffin Bay; Stordal and Wasserburg (1986)), coupled with a fundamental change in the density structure of waters generated in the southern Labrador Sea/open subpolar North Atlantic (i.e. waters from these areas have to be dense enough to reach to a few thousand metres water depth).

4.2. Sources of neodymium to the North Atlantic Ocean

The above discussion highlights that our new data enable a fresh evaluation of potential input sources of Nd to the North Atlantic Ocean. In the following, we will highlight constraints on riverine sources, aeolian inputs, and volcanic inputs, and identify potential areas of boundary exchange.

4.2.1. Inputs and surface water compositions in the subpolar gyre

Significant riverine inputs to the ocean should be readily detectable by decreased salinity in surface water. In the Irminger Basin, we can observe a trend of slightly decreasing salinity following the southwards flow of the Irminger Current (station 2: salinity of 35.13; station 6: salinity of 34.81), which is coupled to a decrease in potential temperature and an increase in oxygen content (Table 2). These properties are in agreement with increased influx of continental-derived water, either as direct riverine water, or as meltwater. Since most of East Greenland is characterised by old bedrock (ε_{Nd} = -40, Revel et al. (1996)), the influx of continental derived water should lead to a shift towards less radiogenic surface seawater along the current. Surface water Nd isotopic compositions show indeed a small decrease along the Irminger Current (station 2: ε_{Nd} = -14.2; station 6: ε_{Nd} = -15.2; Fig. 2, Table 2), pointing to an influx of an unradiogenic source of Nd.

In the region around the Grand Banks, the surface inputs are obvious from elevated Nd concentrations at stations 9 and 13 ([Nd] = 20.6 and 21.1 pmol/kg respectively; Fig. 4d; Table 2), which coincide with lower salinity (34.82 to 35.11; Fig. 3a) and temperature in surface waters, and higher dissolved oxygen levels (Fig. 3a; Table 2). All these features point to an influence from the Labrador Current, which enters the Grand Banks region from the north and encounters remnants of the Gulf Stream in the area of stations 11 and 13 (van Aken,

637 personal communication; Fig. 5). A clear mixing relationship can be observed in the surface
638 water, between modified Gulf Stream water (represented by our results from Station 15;
639 Table 2) and the Labrador Current which is characterised by very different salinities in winter
640 and summer as demonstrated by results from stations SGN5 (a) and Hudson 83-036 LC (b) in
641 Figure 1. Both stations are proximal to each other but were sampled during different times
642 of the year (July for SGN5 and November-December for Hudson-83-036 LC (BIO, 1984);
643 Lacan and Jeandel (2005a); Piepgras and Wasserburg (1987)) and their salinities deviate by
644 2.1 psu, indicating different amounts of freshwater input at different times of the year.
645 Significant changes in salinity are paralleled by significant changes in Nd concentrations. For
646 example, fresher waters at SGN 5 during summer are accompanied by higher Nd
647 concentrations of 43.7 pmol/kg (Lacan and Jeandel, 2005a) compared to concentrations of
648 29.8 pmol/kg in winter (Hudson 83-036 LC; Piepgras and Wasserburg, 1987). These changes
649 in salinity and Nd concentrations are, however, not accompanied by significant changes in
650 the Nd isotopic composition of the Labrador Current (ε_{Nd} = -25 to -26 during both seasons;
651 Piepgras and Wasserburg (1987); Lacan and Jeandel (2005a); (Fig. 9)), pointing to a
652 persistent provenance of the signal from continental North America (Hemming, 2004;
653 Jeandel et al., 2007).

654 Using Equation (2), conservative binary mixing between Gulf Stream water and Labrador
655 Current water can describe the surface water results for the Grand Banks region from this
656 study and previous publications (e.g. Piepgras and Wasserburg, 1987; Mariotti et al., 1988;
657 Lacan and Jeandel, 2005a; Rickli et al., 2009) (Fig. 9). Here, the subscripts 'Mix' refer to the
658 mixture encountered at our stations 9, 11 or 13. SW1 refers to the Labrador Current, which
659 in summer can be described by results from station SGN5 (S = 30.6; ε_{Nd} = -24.9 ± 0.4, [Nd] =
660 43.7 pmol/kg; Lacan and Jeandel (2005a)). The winter composition of the Labrador Current is

represented by S = 32.7; ε_{Nd} = -26.1 ± 0.4, [Nd] = 32.0 pmol/kg, (Hudson 83-036 LC; Piepgras and Wasserburg, 1987). It should be noted that the Nd concentrations and isotopic compositions for this station were derived from unfiltered seawater. The results reported above are therefore recalculated, assuming that only 93% of the total Nd would have been present in dissolved form, following Lacan and Jeandel (2004a). The SW2 refers to the modified Gulf Stream water at station 15 (this study; S = 36.43, ε_{Nd} = -9.9 ± 0.3, [Nd] = 12.1 pmol/kg).

In summary, Nd inputs from Greenland and North America are clearly observable in North Atlantic surface waters, imprinting a rather unradiogenic Nd isotopic composition to large parts of the subpolar gyre (Fig. 5).

4.2.2. Inputs and surface water compositions in the subtropical gyre

Stations investigated in this study from the northern subtropical gyre are more distant from continental sources, and hence less likely to be influenced by direct inputs to the surface waters other than from dust. Neodymium isotopic compositions for surface waters from stations 15 to 21 (Fig.1) reveal a rather uniform Nd isotopic composition for the Gulf Stream of ε_{Nd} = -9.9 to -9.5, a signature also observed for large parts of the subtropical gyre (Fig. 5). A good candidate for setting this signature is African dust, which can have a strong imprint in the western Atlantic Ocean and even in the Caribbean (Measures et al., 2008; Rijkenberg et al., 2014; Kumar et al., 2014). Elevated dissolved Al and Fe concentrations were detected in surface waters from stations 19 to 30 (this study) situated between about 18° to 30°N ([Al] > 30 nmol/dm^3; Rijkenberg et al., 2014; Middag et al., 2015), and Nd isotopic compositions of -11 to -9 are compatible with a strong influence of Saharan dust, characterised by ε_{Nd} ranging from -13.5 to -8.8 in the Caribbean (Kumar et al., 2014).

Therefore, our data set corroborates the idea that the surface waters in the subtropical gyre are influenced by dust inputs, as suggested previously by Tachikawa et al. (1999) and Rickli et al. (2010), and observed by Rijkenberg et al. (2014) and Middag et al. (2015).

In the southern subtropical gyre (stations 25 to 30, Fig. 1, Table 2), surface waters become less salty and warmer towards the south (Fig. 3b), a signature that is coupled with slightly elevated Nd concentrations (17.5 to 22.7 pmol/kg) compared to the stations further north (stations 19 and 21: 13.0 to 13.6 pmol/kg) and slightly less radiogenic Nd isotopic compositions (ε_{Nd} = -10.2 to ε_{Nd} = -10.8; Table 2). Potential candidates for a riverine source of this signature are the Amazon, Orinoco or smaller Caribbean rivers.

The Amazon River has been proposed as an important source of Fe to the study area (Rijkenberg et al., 2014). The Nd characteristics of dissolved Amazon River water are ε_{Nd} = -8.8 ± 0.2 and [Nd] = 850 pmol/kg (AM3-0102, Rousseau et al. (2015)), whereas for the Orinoco River, they are ε_{Nd} = -13.5 ± 0.4 and [Nd] = 57 ± 5 pmol/kg (2sd, n = 4, Osborne et al. (2014)). Due to the prevailing clockwise water flow in the subtropical gyre (Fig. 5), the Nd isotope signature of a potential riverine source from the south would have to be more radiogenic than the values for TTO/TAS station 63 (ε_{Nd} = -13.9 ± 0.5; triangle "g" on Fig. 1, Piepgras and Wasserburg, 1987) or NE Atl E3 O (ε_{Nd} = -12.5 ± 0.4; triangle "h" on Fig. 1, Tachikawa et al., 1999), and for stations 25 to 30 (ε_{Nd} ≈ -10.5). This, therefore, excludes the Orinoco River as a potential source. Concerning the Amazon River, a recent study by Rousseau et al. (2015) shows that dissolved riverine Nd has little influence on the Nd characteristics of the Atlantic Ocean. On the other hand, release of Nd from suspended river sediments is suggested to have a significant impact on the Nd concentration and isotopic composition in the Amazon plume and the open ocean. However, the ε_{Nd} of the Amazon suspended sediment is about -10.7 (Rousseau et al., 2015). This value is similar to the

surface seawater measured at station 30 of the present study (ε_{Nd} = -10.8 ± 0.3, Table 2), and it is less radiogenic than the values at stations 25 and 28 (ε_{Nd} = -10.3 and -10.2 respectively). Therefore, Nd influx from the Amazon River is probably not a good candidate to explain the shift towards more radiogenic Nd values observed at station 30 to station 25.

Another riverine source may be from the Caribbean islands. Indeed, riverine inputs from weathering of these volcanic islands could shift the Nd isotopic composition of the surface waters to more radiogenic values while decreasing salinity. However, to our knowledge, no Nd isotope data are available for any Caribbean island rivers, and therefore this hypothesis remains to be tested.

4.2.3. The role of volcanic ash in surface seawater Nd isotopic compositions

The final candidate for significant input of Nd to the surface ocean in the southern subtropical gyre is volcanic material. This has been suggested as a significant supplier for radiogenic Nd, either via direct aeolian fluxes or via the weathering of volcanic rocks (e.g. Jeandel et al., 1998; Amakawa et al., 2000; Lacan and Jeandel, 2001; Stichel et al., 2012b; Grenier et al., 2013).

The Soufrière Hills volcano, on the Caribbean island of Montserrat, became active in 1995, after having been dormant for centuries. In February 2010, two month before sampling along GEOTRACES section GA02 commenced, an eruption sent large ash clouds eastwards, reaching Antigua and Guadeloupe. The only surface seawater measurement available for Nd in the vicinity of the Caribbean from before 1995 is station OCE 63-3 (triangle f on Figure 1), which features an ε_{Nd} value of -9.6 ± 0.9 (no concentration data available; Piepgras and Wasserburg (1987)). This is somewhat more radiogenic than the surface values determined at stations 25 to 30 (Fig. 5).

In order to assess the potential impact of volcanic activity on seawater Nd, surface seawater was collected under the ash plume of the Eyjafjallajökull 2010 volcanic eruption (Achterberg et al., 2013). Neodymium results for one of these samples from underneath the ash plume (Table 4, RRS Discovery) were compared to surface seawater samples collected during the GA02 cruise south of Iceland, outside the direct influence of the volcanic plume (Table 4, black triangles Fig. 1). Whilst the 'plume' sample has a high Fe concentration due to volcanic material (Achterberg et al., 2013), its Nd isotopic composition and concentration (ε_{Nd} = -13.3 ± 0.3 and [Nd] = 18.2 pmol/kg; Table 4) is identical, within uncertainty, to results obtained for the non-plume surface waters (i.e. ε_{Nd} = -14.2 ± 0.3, [Nd] = 17.3 pmol/kg and ε_{Nd} = -13.0 ± 0.3, [Nd] = 16.9 pmol/kg) and to the overall Nd isotope signature of surface waters from the North Atlantic Subpolar Gyre (see Fig. 5 and Lacan and Jeandel (2004c)). Tephra samples collected from the Eyjafjallajökull eruption in 2010 feature ε_{Nd} values of about +7 (Sigmarsson et al., 2011), and according to experiments performed by Pearce et al. (2013), dissolution of basaltic material should lead to a more radiogenic Nd isotopic composition of seawater within seven days. As our samples were collected about 3 weeks after the first main eruption, the results appear to suggest that volcanic ash had no impact on the Nd signature of surface seawater in this case. A similar conclusion is reached when the surface water samples from stations 25 to 30, in the vicinity of the Caribbean, are considered. These samples were collected in June 2010 (Table 2), about four months after the Soufrière Hills volcano eruption. Volcanic ash from Montserrat can be characterised by an ε_{Nd} of +6.2 ± 0.2 (Kumar et al., 2014). However, surface waters of the area do not show such radiogenic values. We hence conclude that dissolution of volcanic ash appears to have no significant impact on surface water Nd concentrations and isotopic compositions in the

two investigated areas of the Atlantic Ocean. However, future work is needed to fully resolve this question.

4.2.4. Boundary Exchange

Boundary exchange of seawater Nd with continental margins has been shown to take place in several areas of the global ocean (Lacan and Jeandel, 2005a, 2005b; Andersson et al., 2008; Grasse et al., 2012; Jeandel et al., 2013; Grenier et al., 2013). The present data allow the identification of two areas where boundary exchange occurs in the subpolar western North Atlantic Ocean: (i) the Irminger Basin and (ii) the southeastern Labrador Sea & the vicinity of the Grand Banks. Indeed, as suggested above (section 4.1.2), the Nd characteristics determined for NWABW in the subpolar gyre are best explained by such a mechanism. For example, the bottom most samples of the three stations located in the Irminger Sea (stations 2, 5 and 6, Fig. 1) feature the same Nd isotopic composition within error (ε_{Nd} = -11.3 ± 0.6 at station 2, ε_{Nd} = -10.8 ± 0.3 at station 5 and ε_{Nd} = -10.6 ± 0.3 at station 6, Table 2). The Nd concentration at station 2 is 16.2 pmol/kg and similar values are observed at stations 5 and 6 ([Nd] ≈ 15.8 pmol/kg, Table 2). When taking into account the entire NWABW layer, the Nd isotopic compositions are systematically more radiogenic for samples collected closer to the bottom (e.g., station 6: ε_{Nd} = -11.2 ± 0.3 at 3000 m and ε_{Nd} = -10.6 ± 0.3 at 3086 m; Table 2). The Nd concentrations are, however, similar within uncertainties. Surface sediments (carbonate-free, clay size fraction < 2 µm) collected in the Irminger Basin close to stations 5 and 6 (60° N –38° W) feature ε_{Nd} = -7.9 ± 0.2 and [Nd] = 30.33 ppm (Innocent et al., 1997). Therefore, boundary exchange between seawater and surface sediments may explain the shift to more radiogenic Nd values coupled with a lack of

776 variation in Nd concentrations, in agreement with the results of previous Nd studies for the
777 Irminger Basin (Lacan and Jeandel, 2005a, 2005b).

778 ### *4.3. Biogeochemical cycling of neodymium in the water column*

779 The decoupling of seawater Nd isotopes and concentrations, often called the 'Nd
780 paradox' (e.g. Goldstein and Hemming (2003); see also Jeandel et al. (1995, 1998); Lacan and
781 Jeandel (2001)) can also be readdressed with our new data. Considering the dissolved Nd
782 concentrations along GA02, it is striking that they define three general types of profiles (Fig.
783 4).

784 Firstly, stations 2,5,6 in the Irminger Sea show relatively constant Nd concentrations with
785 water depth (e.g. station 2 in Figure 4a; vertical gradient in [Nd] = 2.7 pmol/kg), but Nd
786 isotopic compositions that vary by 4.5 ε-units in the water column. This observation is in
787 agreement with previous studies (Lacan and Jeandel, 2005a).

788 Secondly, surface and subsurface waters in the SE Labrador Sea and around the Grand
789 Banks show elevated Nd concentrations (e.g. Station 9, Fig. 4c), probably associated with
790 increased Nd inputs to this area by the Labrador Current, which ultimately delivers Nd
791 eroded from the North American continent (low ε_{Nd}).

792 Thirdly, a strong vertical gradient of [Nd] in the water column is revealed from about 40°N
793 southwards (Fig. 4e: vertical gradients in [Nd] of up to ~22 pmol/kg), which is decoupled
794 from the equally pronounced structure in the Nd isotopic compositions (vertical gradients of
795 2.6 to 4.3 ε units, Fig. 4). At stations 15 to 30, Nd concentrations are lower in surface waters
796 ([Nd] ≈ 13 pmol/kg), increase linearly to about 1000 m water depth, show constant
797 concentrations at intermediate water depths (1000-3000 m), and increase again towards the
798 bottom ([Nd] ≈ 32 pmol/kg) (Fig. 4e; Table 2). This general pattern in dissolved Nd

799 concentrations with water depths, showing three distinct vertical sections, can be observed
800 over a distance of 3400 km within the western subtropical gyre, meaning that the Nd
801 concentration profiles for stations 15 to 30 are virtually identical (omitting the surface
802 layers; Fig. 4e). This suggests a common mechanism governing Nd cycling in the water
803 column in this region compared to other areas of the global ocean that feature a rather
804 monotonous increase of Nd concentrations with depth (e.g. North Pacific (Piepgras and
805 Jacobsen, 1988; Amakawa et al., 2004), South Pacific (Molina-Kescher et al., 2014), Indian
806 Ocean (Bertram and Elderfield, 1993; Jeandel et al., 1998), Drake Passage (Piepgras and
807 Wasserburg, 1982; Stichel et al., 2012a), South Atlantic (Jeandel, 1993)). The gradient along
808 which Nd concentration increase with depth in the western North Atlantic is 1 pmol/kg per
809 84 m (station 30) to 1 pmol/kg per 220 m (station 19) depth in the upper layer, and 1
810 pmol/kg per 148 m (station 21) to 214 m (station 28) depth in the lower layer (Table 2).
811 Notably, these gradients are higher than observations for the eastern North Atlantic Ocean
812 (e.g. 1 pmol/kg per 208-394 m (Stichel et al., 2015)) and in the Drake Passage (e.g. 1 pmol/kg
813 per 212-359 m (Piepgras and Wasserburg, 1982; Stichel et al., 2012a)).

814 The increase in Nd concentrations in the upper layer of the water column is correlated
815 with decrease in oxygen and an increase in nutrient contents (see Table 2 and Rijkenberg et
816 al., 2014). This 'nutrient-like' behaviour was also observed by Stichel et al. (2015) in the
817 eastern North Atlantic and can be explained by scavenging of Nd onto particles in the
818 (sub)surface and release of previously adsorbed/scavenged Nd from organic particles as they
819 remineralise at depth. Following Stichel et al. (2015), this process can be detected by
820 comparing Nd concentrations with apparent oxygen utilisation (AOU; measure for
821 decomposition of organic matter) (trajectories 'A' and 'B'; Figure 10). However, the amount
822 of Nd released as well as the spread in AOU is much more limited in the western than in the

823 eastern Atlantic Ocean, where atmospheric inputs may be supplying more Nd available for
824 scavenging, and where a pronounced oxygen minimum zone is encountered (Stichel et al.,
825 2015).

826 A common feature between the western and eastern basins is the increasing Nd
827 concentration from about 2500 m depth to the bottom, which is accompanied by relatively
828 constant AOU values (arrow 'D', Fig. 10). We agree with the interpretation of Stichel et al.
829 (2015) that this increased Nd concentration may be associated with dissolution of authigenic
830 coatings from settling particles, which carry a seawater Nd isotopic composition. This
831 reversible scavenging process can be pictured as a rapid exchange process in terms of the
832 isotopic composition, where, in this case, seawater and exchangeable particulate Nd have
833 similar Nd isotopic compositions at a given water depth (Nozaki and Alibo, 2003b). The net
834 increase in concentration hence stems from transport of Nd down the water column, but is
835 not in conflict with the observation of distinct Nd isotopic compositions for various water
836 layers in the same area (Nozaki and Alibo, 2003a; Siddall et al., 2008; Rempfer et al., 2011).

837 The constant Nd concentration from ~1000 m (~500 m at station 30) down to ~2500 –
838 3000 m (Fig. 4e) along section GA02 is accompanied by a 2-3 fold increase in AOU, which
839 yields a distinct flat trend in Figure 10 (arrow "C"). This trend seems unique to the western
840 North Atlantic, where strong lateral advection of deep waters is observed along the western
841 basins. This suggests that high water mass velocities may play a key role in generating the
842 distinctive Nd concentration patterns. This interpretation is supported by the data of Andrié
843 et al. (1997) who performed direct velocity measurements in the Deep Western Boundary
844 Current (DWBC) just to the south of the southernmost profile of the present study, at about
845 7˚N between the coast and 35˚W. These authors show that the upper core of the DWBC has
846 a maximum velocity of more than 40 cm/s at a depth of about 1500 m (Andrié et al., 1997).

847 Furthermore, zonally integrated stream functions calculated from the WOCE hydrography
848 data suggest that the highest mass transport at about 20˚N in the Atlantic Ocean occurs
849 between 1000 and 2000 m depth (Ganachaud, 2003). Therefore, it seems that strong lateral
850 advection keeps Nd concentrations constant in the middle layer. In other words, we suggest
851 that lateral rather than vertical processes dominate the cycling and behaviour of Nd at water
852 column depths of 1000 to 3000 m in the western North Atlantic.

853 Even though Nd concentration characteristics appear to be governed by vertical cycling in
854 the water column, Nd isotopic compositions are still able to fingerprint water mass
855 provenance in the studied area, as shown in previous sections. This suggests that, at least
856 away from continental margins and in strongly advective parts of the ocean, such as the NW
857 Atlantic Ocean, the Nd isotopic composition of seawater is a powerful tracer of modern
858 water masses.

859 **5. Conclusions**

860 New Nd isotopic composition and concentration results are presented for seawater from
861 twelve depth profiles in the north to equatorial western Atlantic Ocean along the
862 GEOTRACES GA02 section. Improved analytical precision for seawater Nd isotope analyses,
863 compared to pioneering studies in the 1980s, allow revisiting and better defining the Nd
864 isotopic composition of NADW and its precursor water masses in the subpolar North Atlantic
865 and evaluating the viability of dissolved Nd isotopes as a water mass tracer.

866 In detail, ULSW carries a very well defined Nd isotopic composition, while the original
867 LSW signature is lost more rapidly during advection away from its source region in the
868 Labrador Sea. The stations of the GA02 section are not well placed to trace NEADW, which is
869 only encountered in diluted form in the Irminger Sea and further downstream in the

subpolar gyre. Resampling of stations in the Irminger Sea however reveals that sediment resuspension and exchange with the continental margin plays an important role in setting the Nd isotopic composition of the denser water masses NEADW and NWABW.

Exported NADW can be separated into upper- and lower-NADW, based on their distinct Nd isotopic compositions. While results for upper-NADW (ε_{Nd} = -13.2 ± 1.0, 2sd, n = 10) show excellent agreement with historical measurements (ε_{Nd} = -13.5 ± 0.5), our data for lower-NADW are more radiogenic (ε_{Nd} = -12.4 ± 0.4, 2sd, n = 16) than published values.

Results for surface seawater provide insight into the predominant continental Nd inputs (riverine/glacial) from Greenland and North America. These contribute to the relatively unradiogenic Nd signature of the subpolar gyre in the North Atlantic. The Nd isotopic fingerprint of the subtropical gyre in contrast is influenced by dust input from Africa. None of the investigated surface waters, including a sample collected in the ash plume of the large 2010 Eyjafjallajökull eruption, provides evidence for significant addition of Nd from volcanic ash to the surface ocean. In contrast, boundary exchange of bottom waters with suspended sediments plays an important role in modifying the bottom water isotopic composition and concentration in areas off Southeastern Greenland (Irminger Sea) and in the vicinity of the Grand Banks (Newfoundland).

Comparing dissolved seawater Nd concentrations and isotopic compositions demonstrate that the two parameters are clearly decoupled. Neodymium concentrations generally increase with depth due to reversible scavenging with a net transport of Nd down the water column. However, in the middle of the water column (1000 – 3000 m), strong lateral advection dominates the cycling of Nd in the western North Atlantic. Ultimately, our

understanding of the vertical cycling of Nd will be greatly aided by future GEOTRACES studies that will investigate the Nd isotopic compositions and concentrations of marine particulates.

In summary, our study clearly supports the conclusion that Nd isotopes can serve as an excellent water mass tracer, if sampled in areas away from oceanic margin, and particularly in areas of strong advection (i.e., deep western boundary current). Our data also indicate that it will be important to more critically assess the composition of northern-sourced Atlantic water masses in the past, as these may have been characterized by different Nd isotopic compositions than in the modern world.

Acknowledgements

The authors would like to thank the scientific party and crew of the RV *Pelagia* 64PE319 and 64PE321. Eric Achterberg and Debbie Hembury are warmly thanked for providing the sample collected under the Eyjafjallajökull volcano plume, and Derek Vance for providing the Nd spike. M. Lambelet would like to thanks all members of the MAGIC group, as well as Maxence Paul, for their support in the lab as well as for constructive discussion about the present data set (particularly T. Stichel, whose comments helped improve an earlier draft of this manuscript). We would like to thank A. Piotrowski, T. Noble and an anonymous reviewer as well as editor A. Bowie for their constructive comments. This work was funded by the NERC project NE/J021636/1.

References

Achterberg E. P., Moore C. M., Henson S. a., Steigenberger S., Stohl A., Eckhardt S., Avendano L. C., Cassidy M., Hembury D., Klar J. K., Lucas M. I., MacEy A. I., Marsay C. M. and Ryan-Keogh T. J. (2013) Natural iron fertilization by the Eyjafjallajökull volcanic eruption. *Geophys. Res. Lett.* **40**, 921–926.

Albarède F. and Goldstein S. L. (1992) World map of Nd isotopes in sea-floor ferromanganese deposits. *Geology* **20**, 761–763.

Alley R. B., Marotzke J., Nordhaus W. D., Overpeck J. T., Peteet D. M., Pielke R. a, Pierrehumbert R. T., Rhines P. B., Stocker T. F., Talley L. D. and Wallace J. M. (2003) Abrupt climate change. *Science* **299**, 2005–2010.

Amakawa H., Alibo D. S. and Nozaki Y. (2000) Nd isotopic composition and REE pattern in the surface waters of the eastern Indian Ocean and its adjacent seas. *Geochim. Cosmochim. Acta* **64**, 1715–1727.

Amakawa H., Nozaki Y., Alibo D. S., Zhang J., Fukugawa K. and Nagai H. (2004) Neodymium isotopic variations in Northwest Pacific waters. *Geochim. Cosmochim. Acta* **68**, 715–727.

Andersson P. S., Porcelli D., Frank M., Björk G., Dahlqvist R. and Gustafsson Ö. (2008) Neodymium isotopes in seawater from the Barents Sea and Fram Strait Arctic–Atlantic gateways. *Geochim. Cosmochim. Acta* **72**, 2854–2867.

Andrié C., Gouriou Y., Bourlès B., Oudot C. and Ternon J. F. (1997) International WOCE Newsletter. *Int. WOCE Newsl.*

Arsouze T., Dutay J.-C., Lacan F. and Jeandel C. (2009) Reconstructing the Nd oceanic cycle using a coupled dynamical – biogeochemical model. *Biogeosciences* **6**, 2829–2846.

de Baar H. J. W., Bacon M. P., Brewer P. G. and Bruland K. W. (1985) Rare earth elements in the Pacific and Atlantic Oceans. *Geochim. Cosmochim. Acta* **49**, 1943–1959.

Basak C., Pahnke K., Frank M., Lamy F. and Gersonde R. (2015) Neodymium isotopic characterization of Ross Sea Bottom Water and its advection through the southern South Pacific. *Earth Planet. Sci. Lett.* **419**, 211–221.

Bertram C. J. and Elderfield H. (1993) The geochemical balance of the rare earth elements and neodymium isotopes in the oceans. *Geochim. Cosmochim. Acta* **57**, 1957–1986.

von Blanckenburg F. (1999) Tracing Past Ocean Circulation? *Sci.* **286** , 1862–1863.

Böhm E., Lippold J., Gutjahr M., Frank M., Blaser P., Antz B., Fohlmeister J., Frank N., Andersen M. B. and Deininger M. (2015) Strong and deep Atlantic meridional overturning circulation during the last glacial cycle. *Nature* **517**, 73–76.

944 Broecker W. (1991) The Great Ocean Conveyor. *Oceanography* **4**, 79–89.

945 Carter P., Vance D., Hillenbrand C. D., Smith J. a. and Shoosmith D. R. (2012) The neodymium
946 isotopic composition of waters masses in the eastern Pacific sector of the Southern
947 Ocean. *Geochim. Cosmochim. Acta* **79**, 41–59.

948 Copard K., Colin C., Frank N., Jeandel C., Montero-Serrano J.-C., Reverdin G. and Ferron B.
949 (2011) Nd isotopic composition of water masses and dilution of the Mediterranean
950 outflow along the southwest European margin. *Geochemistry, Geophys. Geosystems* **12**,
951 1–14.

952 Crocket K. C., Lambelet M., van de Flierdt T., Rehkämper M. and Robinson L. F. (2014)
953 Measurement of fossil deep-sea coral Nd isotopic compositions and concentrations by
954 TIMS as NdO+, with evaluation of cleaning protocols. *Chem. Geol.* **374-375**, 128–140.

955 Dickson R. R. and Brown J. (1994) The production of North Atlantic Deep Water : sources,
956 rates, and pathways. *J. Geophys. Res.* **99**, 12319–12341.

957 Elderfield H. and Greaves M. J. (1982) The rare earth elements in seawater. *Nature* **296**, 214–
958 219.

959 Elderfield H., Whitfield M., Burton J. D., Bacon M. P. and Liss P. S. (1988) The oceanic
960 chemistry of the rare-earth elements. *Philos. Trans. R. Soc. London* **325**, 105–126.

961 van de Flierdt T. and Frank M. (2010) Neodymium isotopes in paleoceanography. *Quat. Sci.*
962 *Rev.* **29**, 2439–2441.

963 van de Flierdt T., Pahnke K., Amakawa H., Andersson P., Basak C., Coles B., Colin C., Crocket
964 K., Frank M., Frank N., Goldstein S. L., Goswami V., Haley B. A., Hathorne E. C., Hemming
965 S. R., Henderson G. M., Jeandel C., Jones K., Kreissig K., Lacan F., Lambelet M., Martin E.
966 E., Newkirk D. R., Obata H., Pena L., Piotrowski A. M., Pradoux C., Scher H. D., Schöberg
967 H., Singh S. K., Stichel T., Tazoe H., Vance D. and Yang J. (2012) GEOTRACES
968 intercalibration of neodymium isotopes and rare earth element concentrations in
969 seawater and suspended particles. Part 1: reproducibility of results for the international
970 intercomparison. *Limnol. Oceanogr. Methods* **10**, 234–251.

971 Frank M. (2002) Radiogenic isotopes: tracers of past ocean circulation and erosional input.
972 *Rev. Geophys.* **40**, 1–38.

973 Ganachaud A. (2003) Large-scale mass transports, water mass formation, and diffusivities
974 estimated from World Ocean Circulation Experiment (WOCE) hydrographic data. *J.*
975 *Geophys. Res.* **108**.

976 Ganachaud A. and Wunsch C. (2000) Improved estimates of global ocean circulation, heat
977 transport and mixing from hydrographic data. *Nature* **408**, 453–457.

978 Garcia-Solsona E., Jeandel C., Labatut M., Lacan F., Vance D., Chavagnac V. and Pradoux C.

(2014) Rare earth elements and Nd isotopes tracing water mass mixing and particle-seawater interactions in the SE Atlantic. *Geochim. Cosmochim. Acta* **125**, 351–372.

Gault-Ringold M. and Stirling C. H. (2012) Anomalous isotopic shifts associated with organic resin residues during cadmium isotopic analysis by double spike MC-ICPMS. *J. Anal. At. Spectrom.* **27**, 449–459.

Godfrey L. V., Zimmermann B., Lee D.-C., King R. L., Vervoort J. D., Sherrell R. M. and Halliday a. N. (2009) Hafnium and neodymium isotope variations in NE Atlantic seawater. *Geochemistry, Geophys. Geosystems* **10**, 1–13.

Goldstein S. and Hemming S. (2003) Long-lived isotopic tracers in oceanography, paleoceanography, and ice-sheet dynamics. *Treatise on geochemistry*.

Goldstein S. L., O'Nions R. K. and Hamilton P. J. (1984) A Sm-Nd isotopic study of atmospheric dusts and particulates from major river systems. *Earth Planet. Sci. Lett.* **70**, 221–236.

Grasse P., Stichel T., Stumpf R., Stramma L. and Frank M. (2012) The distribution of neodymium isotopes and concentrations in the Eastern Equatorial Pacific: Water mass advection versus particle exchange. *Earth Planet. Sci. Lett.* **353-354**, 198–207.

Grenier M., Jeandel C., Lacan F., Vance D., Venchiarutti C., Cros A. and Cravatte S. (2013) From the subtropics to the central equatorial Pacific Ocean: Neodymium isotopic composition and rare earth element concentration variations. *J. Geophys. Res. Ocean.* **118**, 592–618.

Haley B. A., Frank M., Hathorne E. and Pisias N. (2014) Biogeochemical implications from dissolved rare earth element and Nd isotope distributions in the Gulf of Alaska. *Geochim. Cosmochim. Acta* **126**, 455–474.

Hanawa K. and Talley L. D. (2001) Mode Waters. In *Ocean circulation and climate* pp. 373–386.

Hemming S. R. (2004) Heinrich Events: massive late pleistocene detritus layers of the North Atlantic and their global climate imprint. *Rev. Geophys.* **42**, 1–43.

Huang K.-F., Oppo D. W. and Curry W. B. (2014) Decreased influence of Antarctic intermediate water in the tropical Atlantic during North Atlantic cold events. *Earth Planet. Sci. Lett.* **389**, 200–208.

Innocent C., Fagel N., Stevenson R. K. and Hillaire-Marcel C. (1997) Sm-Nd signature of modern and late Quaternary sediments from the northwest North Atlantic: Implications for deep current changes since the Last Glacial Maximum. *Earth Planet. Sci. Lett.* **146**, 607–625.

Jacobsen S. B. and Wasserburg G. J. (1980) Sm-Nd evolution of chondrites. *Earth Planet. Sci.*

1014 *Lett.* **50**, 139–155.

1015 Jeandel C. (1993) Concentration and isotopic composition of Nd in the South Atlantic Ocean.
1016 *Earth Planet. Sci. Lett.* **117**, 581–591.

1017 Jeandel C., Arsouze T., Lacan F., Techine P. and Dutay J. (2007) Isotopic Nd compositions and
1018 concentrations of the lithogenic inputs into the ocean: A compilation, with an emphasis
1019 on the margins. *Chem. Geol.* **239**, 156–164.

1020 Jeandel C., Bishop J. K. and Zindler A. (1995) Exchange of neodymium and its isotopes
1021 between seawater and small and large particles in the Sargasso Sea. *Geochim.*
1022 *Cosmochim. Acta* **59**, 535–547.

1023 Jeandel C., Delattre H., Grenier M., Pradoux C. and Lacan F. (2013) Rare earth element
1024 concentrations and Nd isotopes in the Southeast Pacific Ocean. *Geochemistry, Geophys.*
1025 *Geosystems* **14**, 1–14.

1026 Jeandel C., Thouron D. and Fieux M. (1998) Concentrations and isotopic compositions of
1027 neodymium in the eastern Indian Ocean and Indonesian straits. *Geochim. Cosmochim.*
1028 *Acta* **62**, 2597–2607.

1029 Kieke D., Klein B., Stramma L., Rhein M. and Koltermann K. P. (2009) Variability and
1030 propagation of Labrador Sea Water in the southern subpolar North Atlantic. *Deep. Res. I*
1031 **56**, 1656–1674.

1032 Kieke D., Rhein M., Stramma L., Smethie W. M., LeBel D. A. and Zenk W. (2006) Changes in
1033 the CFC Inventories and Formation Rates of Upper Labrador Sea Water, 1997 – 2001. *J.*
1034 *Phys. Oceanogr.* **36**, 64–86.

1035 Kumar A., Abouchami W., Galer S. J. G., Garrison V. H., Williams E. and Andreae M. O. (2014)
1036 A radiogenic isotope tracer study of transatlantic dust transport from Africa to the
1037 Caribbean. *Atmos. Environ.* **82**, 130–143.

1038 Lacan F. and Jeandel C. (2005a) Acquisition of the neodymium isotopic composition of the
1039 North Atlantic Deep Water. *Geochemistry, Geophys. Geosystems* **6**, 1–20.

1040 Lacan F. and Jeandel C. (2004a) Denmark Strait water circulation traced by heterogeneity in
1041 neodymium isotopic compositions. *Deep Sea Res. Part I Oceanogr. Res. Pap.* **51**, 71–82.

1042 Lacan F. and Jeandel C. (2005b) Neodymium isotopes as a new tool for quantifying exchange
1043 fluxes at the continent–ocean interface. *Earth Planet. Sci. Lett.* **232**, 245–257.

1044 Lacan F. and Jeandel C. (2004b) Neodymium isotopic composition and rare earth element
1045 concentrations in the deep and intermediate Nordic Seas: Constraints on the Iceland
1046 Scotland Overflow Water signature. *Geochemistry, Geophys. Geosystems* **5**, 10.

1047 Lacan F. and Jeandel C. (2004c) Subpolar Mode Water formation traced by neodymium

isotopic composition. *Geophys. Res. Lett.* **31**, 5.

Lacan F. and Jeandel C. (2001) Tracing Papua New Guinea imprint on the central Equatorial Pacific Ocean using neodymium isotopic compositions and Rare Earth Element patterns. *Earth Planet. Sci. Lett.* **186**, 497–512.

Lacan F., Tachikawa K. and Jeandel C. (2012) Neodymium isotopic composition of the oceans: A compilation of seawater data. *Chem. Geol.* **300-301**, 177–184.

Latremouille M. P. (1984) *Bio Review '84, Bedford Institute of Oceanography*., Dartmouth, Nova Scotia.

Lavender K. L., Davis R. E. and Owens W. B. (2000) Mid-depth recirculation observed in the interior Labrador and Irminger seas by direct velocity measurements. *Nat. (Letters to)* **407**, 66–69.

Mariotti A., Landreau A. and Simon B. (1988) 15N isotope biogeochemistry and natural denitrification process in groundwater: Application to the chalk aquifer of northern France. *Geochim. Cosmochim. Acta* **52**, 1869–1878.

Marshall J. and Speer K. (2012) Closure of the meridional overturning circulation through Southern Ocean upwelling. *Nat. Geosci.* **5**, 171–180.

Mawji E., Schlitzer R., Masferrer E., Abadie C., Abouchami W., Anderson R. F., Baars O., Bakker K., Baskaran M., Bates N. R., Bluhm K., Bowie A., Bown J., Boye M., Boyle E. A., Branellec P., Bruland K. W., Brzezinski M. A., Bucciarelli E., Buesseler K., Butler E., Cai P., Cardinal D., Casciotti K., Chaves J., Cheng H., Chever F., Church T. M., Colman A. S., Conway T. M., Croot P. L., Cutter G. A., Baar H. J. W. De, Souza G. F. De, Dehairs F., Deng F., Thi H., Dulaquais G., Echegoyen-sanz Y., Edwards R. L., Fahrbach E., Fitzsimmons J., Fleisher M., Frank M., Friedrich J., Fripiat F., Galer S. J. G., Gamo T., Garcia E., Gerringa L. J. A., Marcus J., Gonzalez S., Grossteffan E., Hatta M., Hayes C. T., Iris M., Henderson G., Huang K., Jeandel C., Jenkins W. J., John S., Kenna T. C., Klunder M., Kretschmer S., Kumamoto Y., Laan P., Labatut M., Lacan F., Lam P. J., Lannuzel D., Lechtenfeld O. J., Lohan M. C., Lu Y., Masqué P., Mcclain C. R., Measures C., Middag R., Moffett J., Navidad A., Nishioka J., Noble A., Obata H., Ohnemus D. C., Owens S., Planchon F., Pradoux C., Puigcorbé V., Quay P., Radic A., Rehkämper M., Remenyi T., Rijkenberg M. J. A., Rintoul S., Robinson L. F., Roeske T., Rosenberg M., Rutgers M., Loeff V. Der, Ryabenko E., Saito M. A., Roshan S., Salt L., Sarthou G., Schauer U., Scott P., Sedwick P. N., Sha L., Shiller A. M., Sigman D. M., Smethie W., Smith G. J., Sohrin Y., Speich S., Stichel T., Stutsman J., Swift J. H., Tagliabue A., Thomas A., Tsunogai U., Twining B. S., Aken H. M. Van, Heuven S. Van, Ooijen J. Van, Weerlee E. Van, Venchiarutti C., Voelker A. H. L., Wake B., Warner M. J., Woodward E. M. S., Wu J., Wyatt N., Yoshikawa H., Zheng X., Xue Z., Zieringer M. and Zimmer L. A. (2015) The GEOTRACES Intermediate Data Product 2014 The GEOTRACES Group. *Mar. Chem.*, 1–8.

McCartney M. S. and Talley L. D. (1982) The Subpolar Mode Water of the North Atlantic Ocean.pdf. *J. Phys. Oceanogr.* **12**, 1169–1188.

McLennan S. M., Taylor S. R., McCulloch M. T. and Maynard J. B. (1990) Geochemical and Nd-Sr isotopic composition of deep-sea turbidites: Crustal evolution and plate tectonic associations. *Geochim. Cosmochim. Acta* **54**, 2015–2050.

Measures C. I., Henderson G. M., Anderson R. F., Adkins J., Andersson P., Boyle E. A., Cutter G., de Baar H. J. W., Eisenhauer A., Frank M., Francois R., Orians K., Gamo T., German C., Jenkins W., Moffett J., Jeandel C., Jickells T., Krishnaswami S., Mackey D., Masque P., Moore J. K., Oschlies A., van der Loeff M. R., Sharma M., von Damm K. and Zhang J. (2007) GEOTRACES – An international study of the global marine biogeochemical cycles of trace elements and their isotopes. *Chemie der Erde - Geochemistry* **67**, 85–131.

Measures C. I., Landing W. M., Brown M. T. and Buck C. S. (2008) High-resolution Al and Fe data from the Atlantic Ocean CLIVAR-CO2 Repeat Hydrography A16N transect: Extensive linkages between atmospheric dust and upper ocean geochemistry. *Global Biogeochem. Cycles* **22**, 1–10.

Middag R., van Hulten M. M. P., van Aken H. M., Rijkenberg M. J. A., Gerringa L. J. A., Laan P. and de Baar H. J. W. (2015) Dissolved aluminium in the ocean conveyor of the West Atlantic Ocean : Effects of the biological cycle , scavenging , sediment resuspension and hydrography. *Mar. Chem.* **In Press**.

Molina-Kescher M., Frank M. and Hathorne E. (2014) South Pacific dissolved Nd isotope compositions and rare earth element distributions: Water mass mixing versus biogeochemical cycling. *Geochim. Cosmochim. Acta* **127**, 171–189.

Nozaki Y. and Alibo D. S. (2003a) Dissolved rare earth elements in the Southern Ocean, southwest of Australia: Unique patterns compared to the South Atlantic data. *GEOCHEMICAL JOURNAL-JAPAN-* **37**, 47–62.

Nozaki Y. and Alibo D. S. (2003b) Importance of vertical geochemical processes in controlling the oceanic profiles of dissolved rare earth elements in the northeastern Indian Ocean. *Earth Planet. Sci. Lett.* **205**, 155–172.

Oka A., Hasumi H., Obata H., Gamo T. and Yamanaka Y. (2009) Study on vertical profiles of rare earth elements by using an ocean general circulation model. *Global Biogeochem. Cycles* **23**, 1–16.

Orsi A. H., Johnson G. C. and Bullister J. L. (1999) Circulation, mixing, and production of Antarctic Bottom Water. *Prog. Oceanogr.* **43**, 55–109.

Orsi A. H., Smethie W. M. and Bullister J. L. (2002) On the total input of Antarctic waters to the deep ocean : A preliminary estimate from chlorofluorocarbon measurements. *J. Geophys. Res.* **107**, 1–17.

Osborne A. H., Haley B. a., Hathorne E. C., Flögel S. and Frank M. (2014) Neodymium isotopes and concentrations in Caribbean seawater: Tracing water mass mixing and continental input in a semi-enclosed ocean basin. *Earth Planet. Sci. Lett.* **406**, 174–186.

Pahnke K., van de Flierdt T., Jones K. M., Lambelet M., Hemming S. R. and Goldstein S. L. (2012) GEOTRACES intercalibration of neodymium isotopes and rare earth element concentrations in seawater and suspended particles. Part 2: Systematic tests and baseline profiles. *Limnol. Oceanogr. Methods* **10**, 252–269.

Pearce C. R., Jones M. T., Oelkers E. H., Pradoux C. and Jeandel C. (2013) The effect of particulate dissolution on the neodymium (Nd) isotope and Rare Earth Element (REE) composition of seawater. *Earth Planet. Sci. Lett.* **369-370**, 138–147.

Piepgras D. . and Wasserburg G. . (1987) Rare earth element transport in the western North Atlantic inferred from Nd isotopic observations. *Geochim. Cosmochim. Acta* **51**, 1257–1271.

Piepgras D. J. and Jacobsen S. B. (1988) The isotopic composition of neodymium in the North Pacific. *Geochim. Cosmochim. Acta* **52**, 1373–1381.

Piepgras D. J. and Wasserburg G. J. (1983) Influence of Mediterranean outflow on the isotopic composition of neodymium in waters of the North Atlantic. *J. Geophys. Res.* **88**, 5997–6006.

Piepgras D. J. and Wasserburg G. J. (1982) Isotopic Composition of Neodymium in Waters from the Drake Passage. *Science (80-.).* **217**, 207–214.

Piepgras D. J., Wasserburg G. J. and Dasch E. J. (1979) The isotopic composition of Nd in different ocean masses. *Earth Planet. Sci. Lett.* **45**, 223–236.

Rahmstorf S. (2002) Ocean circulation and climate during the past 120,000 years. *Nature* **419**, 207–214.

Rempfer J., Stocker T. F., Joos F., Dutay J.-C. and Siddall M. (2011) Modelling Nd-isotopes with a coarse resolution ocean circulation model: Sensitivities to model parameters and source/sink distributions. *Geochim. Cosmochim. Acta* **75**, 5927–5950.

Revel M., Sinko J. A., Grousset F. E. and Biscaye P. E. (1996) Sr and Nd isotopes as tracers of North Atlantic lithic particles: Paleoclimatic implications. *Paleoceanography* **11**, 95–113.

Rhein M., Kieke D., Hüttl-Kabus S., Roessler A., Mertens C., Meissner R., Klein B., Böning C. W. and Yashayaev I. (2011) Deep water formation, the subpolar gyre, and the meridional overturning circulation in the subpolar North Atlantic. *Deep Sea Res. Part II Top. Stud. Oceanogr.* **58**, 1819–1832.

Rhein M., Kieke D. and Steinfeldt R. (2015) Advection of North Atlantic Deep Water fromthe Labrador Sea to the southern hemisphere. *J. Geophys. Res.* **120**, 1–17.

1156 Rickli J., Frank M., Baker a. R., Aciego S., de Souza G., Georg R. B. and Halliday a. N. (2010)
1157 Hafnium and neodymium isotopes in surface waters of the eastern Atlantic Ocean:
1158 Implications for sources and inputs of trace metals to the ocean. *Geochim. Cosmochim.*
1159 *Acta* **74**, 540–557.

1160 Rickli J., Frank M. and Halliday A. N. (2009) The hafnium–neodymium isotopic composition of
1161 Atlantic seawater. *Earth Planet. Sci. Lett.* **280**, 118–127.

1162 Rickli J., Gutjahr M., Vance D., Fischer-Gödde M., Hillenbrand C.-D. and Kuhn G. (2014)
1163 Neodymium and hafnium boundary contributions to seawater along the West Antarctic
1164 continental margin. *Earth Planet. Sci. Lett.* **394**, 99–110.

1165 Rijkenberg M. J. A., Middag R., Laan P., Gerringa L. J. S., van Aken H. M., Schoemann V., de
1166 Jong J. T. M. and de Baar H. J. W. (2014) The distribution of dissolved iron in the West
1167 Atlantic Ocean. *PLoS One* **9**, e101323.

1168 Roberts N. L., Piotrowski A. M., McManus J. F. and Keigwin L. D. (2010) Synchronous
1169 deglacial overturning and water mass source changes. *Science* **327**, 75–8.

1170 Rousseau T. C. C., Sonke J. E., Chmeleff J., van Beek P., Souhaut M., Boaventura G., Seyler P.
1171 and Jeandel C. (2015) Rapid neodymium release to marine waters from lithogenic
1172 sediments in the Amazon estuary. *Nat. Commun.* **6**, 7592.

1173 Schlitzer R. (2012) Ocean Data View.

1174 Schmitz W. J. (1996) *On the world ocean circulation: Volume I*., Massachusetts.

1175 Shabani M. B., Akagi T. and Masuda A. (1992) Preconcentration of trace rare-earth elements
1176 in seawater by complexation with bis(2-ethylhexyl) hydrogen phosphate and 2-
1177 ethylhexyl dihydrogen phosphate adsorbed on a C18 cartridge and determination by
1178 inductively coupled plasma mass spectrometry. *Anal. Chem.* **64**, 737–743.

1179 Siddall M., Khatiwala S., van de Flierdt T., Jones K., Goldstein S. L., Hemming S. and Anderson
1180 R. F. (2008) Towards explaining the Nd paradox using reversible scavenging in an ocean
1181 general circulation model. *Earth Planet. Sci. Lett.* **274**, 448–461.

1182 Sigmarsson O., Vlastelic I., Andreasen R., Bindeman I., Devidal J.-L., Moune S., Keiding J. K.,
1183 Larsen G., Höskuldsson a. and Thordarson T. (2011) Remobilization of silicic intrusion
1184 by mafic magmas during the 2010 Eyjafjallajökull eruption. *Solid Earth* **2**, 271–281.

1185 Singh S. P., Singh S. K., Goswami V., Bhushan R. and Rai V. K. (2012) Spatial distribution of
1186 dissolved neodymium and εNd in the Bay of Bengal: Role of particulate matter and
1187 mixing of water masses. *Geochim. Cosmochim. Acta* **94**, 38–56.

1188 Smethie W. M., Fine R. A., Putzka A. and Jones P. E. (2000) Tracing the flow of North Atlantic
1189 Deep Water using chlorofiuorocarbons. *J. Geophys. Res.* **105**, 14297–14323.

1190 Spivack A. J. and Wasserburg G. J. (1988) Neodymium isotopic composition of the
1191 Mediterranean outflow and the eastern North Atlantic. *Geochim. Cosmochim. Acta* **52**,
1192 2767–2773.

1193 Steinfeldt R. and Rhein M. (2004) Spreading velocities and dilution of North Atlantic Deep
1194 Water in the tropical Atlantic based on CFC time series. *J. Geophys.* **109**, 1–15.

1195 Stichel T., Frank M., Rickli J. and Haley B. A. (2012) The hafnium and neodymium isotope
1196 composition of seawater in the Atlantic sector of the Southern Ocean. *Earth Planet. Sci.*
1197 *Lett.* **317-318**, 282–294.

1198 Stichel T., Frank M., Rickli J., Hathorne E. C., Haley B. A., Jeandel C. and Pradoux C. (2012)
1199 Sources and input mechanisms of hafnium and neodymium in surface waters of the
1200 Atlantic sector of the Southern Ocean. *Geochim. Cosmochim. Acta* **94**, 22–37.

1201 Stichel T., Hartman A. E., Duggan B., Goldstein S. L., Scher H. D. and Pahnke K. (2015)
1202 Separating biogeochemical cycling of neodymium from water mass mixing in the
1203 Eastern North Atlantic. *Earth Planet. Sci. Lett.* **412**, 245–260.

1204 Stordal M. C. and Wasserburg G. J. (1986) Neodymium isotopic study of Baffin Bay water :
1205 sources of REE from very old terranes. *Earth Planet. Sci. Lett.* **77**, 259–272.

1206 Stramma L., Kieke D., Rhein M., Schott F., Yashayaev I. and Koltermann K. P. (2004) Deep
1207 water changes at the western boundary of the subpolar North Atlantic during 1996 to
1208 2001. *Deep Sea Res. I* **51**, 1033–1056.

1209 Stramma L. and Siedler G. (1988) Seasonal Changes in the North Atlantic Subtropical Gyre. *J.*
1210 *Geophys. Res.* **93**, 8111–8118.

1211 Swift J. H. (1984) The circulation of the Denmark Strait and Iceland-Scotland overflow waters
1212 in the North Atlantic. *Deep Sea Res.* **31**, 1339–1355.

1213 Sy A., Rhein M., Lazier J. R. N., Koltermann K. P., Meincke J., Putzka A. and Bersch M. (1997)
1214 Surprisingly rapid spreading of newly formed intermediate waters across the North
1215 Atlantic Ocean. *Nature* **386**, 675–679.

1216 Tachikawa K., Jeandel C. and Roy-Barman M. (1999) A new approach to the Nd residence
1217 time in the ocean: the role of atmospheric inputs. *Earth Planet. Sci. Lett.* **170**, 433–446.

1218 Talley L. D. and McCartney M. S. (1982) Distribution and circulation of Labrador Sea Water. *J.*
1219 *Phys. Oceanogr.* **12**, 1189–1205.

1220 Tanaka T., Togashi S., Kamioka H., Amakawa H., Kagami H., Hamamoto T., Yuhara M.,
1221 Orihashi Y., Yoneda S., Shimizu H., Kunimaru T., Takahashi K., Yanagi T., Nakano T.,
1222 Fujimaki H., Shinjo R., Asahara Y., Tanimizu M. and Dragusanu C. (2000) JNdi-1: a
1223 neodymium isotopic reference in consistency with LaJolla neodymium. *Chem. Geol.*
1224 **168**, 279–281.

1225 Tomczak M. (2001) Hydrology of the Atlantic Ocean. In *Regional Oceanography* pp. 253 –
1226 270.

1227 Wilson D. J., Crocket K. C., van de Flierdt T., Robinson L. F. and Adkins J. F. (2014) Dynamic
1228 intermediate ocean circulation in the North Atlantic during Heinrich Stadial 1: A
1229 radiocarbon and neodymium isotope perspective. *Paleoceanography* **29**, 1072–1093.

1230 Worthington L. V (1959) The 18° water in the Sargasso Sea. *Deep Sea Res.* **5**, 297–305.

1231 Yashayaev I. and Loder J. W. (2009) Enhanced production of Labrador Sea Water in 2008.
1232 *Geophys. Res. Lett.* **36**, 1–7.

1233

1234 **Figure captions**

1235

1236 **Figure 1:** Map of the North Atlantic Ocean indicating the location of seawater profiles
1237 (black dots with numbers) and surface samples (black triangles) from this study and the
1238 literature (white and grey symbols). White triangles with letters refer to stations from the
1239 literature, the data from which are used for comparison in this study. a: Signature station 5
1240 (Lacan and Jeandel, 2005a); b: Hudson 83-036 LC (Piepgras and Wasserburg, 1987); c:
1241 Thalahassa station 15 (Rickli et al., 2009); d: Hudson 83-036 station 11 (Piepgras and
1242 Wasserburg, 1987); e: Signature station 6 (Lacan and Jeandel, 2005a); f: OCE 63 station 3
1243 (Piepgras and Wasserburg, 1987); g: TTO/TAS station 63 (Piepgras and Wasserburg, 1987); h:
1244 NE Atl. E3 O (Tachikawa et al., 1999). Light grey dots represent literature data where at least
1245 three depths were sampled for Nd isotopic compositions, and the white dots mark stations
1246 with less than three published depths results.

1247 Pink (thicker) arrows represent schematically the spreading of Labrador Sea Water (LSW).
1248 Blue (thinner) arrows symbolise overflow of waters from the Greenland and Norwegian Seas
1249 (DSOW: Denmark Strait Overflow Water; ISOW: Iceland-Scotland Overflow Water). Yellow
1250 (thicker) arrows represent the spreading of North Atlantic Deep Water (NADW) once
1251 exported from the subpolar gyre. Orange (thinner) arrows mark the northward flow of
1252 southern-derived water masses (w-LDW and e-LDW: western and eastern Lower Deep
1253 Water, respectively). Dotted grey lines represent deep recirculation cells. DS: Denmark
1254 Strait; I-F ridge: Iceland Faroe ridge; F-B channel: Faroe Bank channel; CGFZ: Charlie Gibbs
1255 Fracture Zone. Stippled black line marks the path of the section view shown in Figure 2. The
1256 map was created using ODV software, available at http://odv.awi.de/ (Schlitzer, 2012).

Figure 2: Sections of (a) neodymium isotopic composition and (b) neodymium concentrations for the north to equatorial western Atlantic Ocean. For comparison, panel (c) features the salinity results based on the full sample set from the northern part of the GA02 GEOTRACES section. The black lines on panels a and c are the isopycnals σ_θ 27.68, 27.74, 27.81 and 27.88 kg/m^3 defining major water mass boundaries (see Results section and Table 2 for further details); the black lines on panel b are isolines for the apparent oxygen utilisation (AOU, µmol/kg). The black dots represent the location of actual samples which were analysed for neodymium, and the numbers above the upper panel denote the station numbers. Note that only data from this study were utilised. These sections were created with the ODV software (Schlitzer, 2012).

Figure 3: Potential temperature vs salinity diagrams for subpolar (a and c) and subtropical (b and d) stations of the present study. Panels (c) and (d) are enlargements of panels (a) and (b), respectively, to better illustrate intermediate water masses. ULSW: Upper Labrador Sea Water; LSW: Labrador Sea Water; NEADW: North East Atlantic Deep Water; NWABW: North West Atlantic Bottom Water; modified AABW: modified Antarctic Bottom Water. U-NADW: Upper North Atlantic Deep Water; L-NADW: Lower North Atlantic Deep Water. These diagrams were realised using the ODV software (Schlitzer, 2012).

Figure 4: Neodymium concentration (a, c and e) and Nd isotopic composition (b, d and f) depth profiles for the different North Atlantic regions discussed in this study: Irminger Sea (a and b), stations around the Grand Banks (c and d), and Sargasso Sea (e and f). The vertical

dashed line in (f) highlights the often cited value for NADW (ε_{Nd} = -13.5; Piepgras and Wasserburg, 1987). Note the different scale on the x axis of panel (f). Error bars represent the external 2 sigma error for repeat measurement of an in-house seawater sample ([Nd] = ±0.6 pmol/kg and ε_{Nd} = ±0.3, n= 5). If internal errors are larger than external ones these are reported (see Table 2). This applies to all Figures that show uncertainties on measured Nd concentrations and isotopic compositions.

Figure 5: Neodymium isotopic composition for the surface most samples (max depth = 100 m) of the present study (dots with black rim). The arrows represent surface currents (dashed lines for colder waters). The approximate Nd isotopic signature of the continents is depicted with coloured outlines of the coastlines. Map drawn after Schmitz (1996). Literature values are shown as dots without a black rim. Current name abbreviations: CC: Canary Current; EGC: East Greenland Current; FC: Florida Current; GS: Gulf Stream; IC: Irminger Current; LC: Labrador Current; NAC: North Atlantic Current; NC: Norwegian Current; NEC: North Equatorial Current; WGC: Western Greenland Current. This map was realised using the ODV software (Schlitzer, 2012).

Figure 6: Neodymium isotope ratios versus (a) salinity and (b) silicate concentrations. The grey lines show the mixing envelope between a northern end-member (ε_{Nd} ≈ -13.5, S ≈ 34.95 and [SiO_2] ≈ 12 µmol/kg) and a southern end-member (ε_{Nd} ≈ -8.5, S ≈ 34.65 and [SiO_2] ≈ 125 µmol/kg) after Goldstein and Hemming (2003). Subpolar stations from this study: 2, 5, 6, 9, 11 and 13; subtropical stations: 15, 19, 21, 25, 28 and 30. Neodymium data sources: Piepgras and Wasserburg (1983; 1987); Spivack and Wasserburg (1988); Jeandel (1993); Lacan and

Jeandel (2005a); Rickli et al. (2009); Godfrey et al. (2009); Copard et al. (2011); Pahnke et al. (2012); Garcia-Solsona et al. (2014); Stichel et al. (2015). Note that data from the Mediterranean Sea, the Nordic Sea and Baffin Bay were not included.

Figure 7: Neodymium isotopic composition (a and c) and Nd concentrations (b and d) versus neutral density. Panels (a) and (b) show data for neutral densities higher or equal to 27.8 kg/m^3, corresponding to ULSW lower boundary. Panels (c) and (d) are enlargements of panels (a) and (b) respectively, for neutral densities higher or equal to 28.1 kg/m^3, to better illustrate NWABW and modified AABW. Grey shadings delimit the water masses boundaries, and the colour coding represents the different North Atlantic regions discussed in this study: Irminger Sea (green), stations around the Grand Banks (orange), and Sargasso Sea (blue).

Figure 8: CFC-11 concentration section for the north to equatorial western Atlantic Ocean (this study). The black lines contour the Nd isotopic compositions, the locations of which are indicated by black dots. Note that CFCs were determined on 34 stations and on 20 water depths in the same area, compared to the more sparse resolution of the Nd data. This section was realised with the ODV software (Schlitzer, 2012).

Figure 9: Neodymium isotopic composition versus salinity for surface samples in the southern Labrador Sea and in the vicinity of the Grand Banks. Grey symbols are data from the present study, and open symbols are data taken from the literature (Lacan and Jeandel (2005a): SGN 5 (a) and SGN 6 (e); Piepgras and Wasserburg (1987): Hudson 83-036 LC (b) and Hudson 83-06 stn 11 (d); Rickli et al. (2009): Thalahassa 15 (c)). For location of samples

see Figure 1. For details on calculations and endmembers used refer to the main text. The grey areas represent the calculated mixing lines between Gulf Stream and Labrador Current in summer (dark grey) and winter (light grey) respectively.

Figure 10: Neodymium concentration versus apparent oxygen utilisation for the stations from the subtropical western North Atlantic (coloured dots = results from this study). The colour coding represents water depth. Arrows with letters represent different behaviours of Nd in the water column. A: scavenging of surface Nd (stations 25 to 30); B: release of scavenged Nd due to remineralisation of biogenic particles in the upper water column (down to about 500 m depth); C: constant Nd concentration (1000 to 2500 m depth); D: steady increase of Nd, from about 3000 m down to the bottom. For ease of comparison, the same arrows and letter coding has been used as in Stichel et al. (2015), except for the letter C, which marks a different behaviour in the western North Atlantic compared to the eastern basin. Results from the eastern North Atlantic (Stichel et al., 2015) are shown as grey dots. Plot made with the ODV software (Schlitzer, 2012).

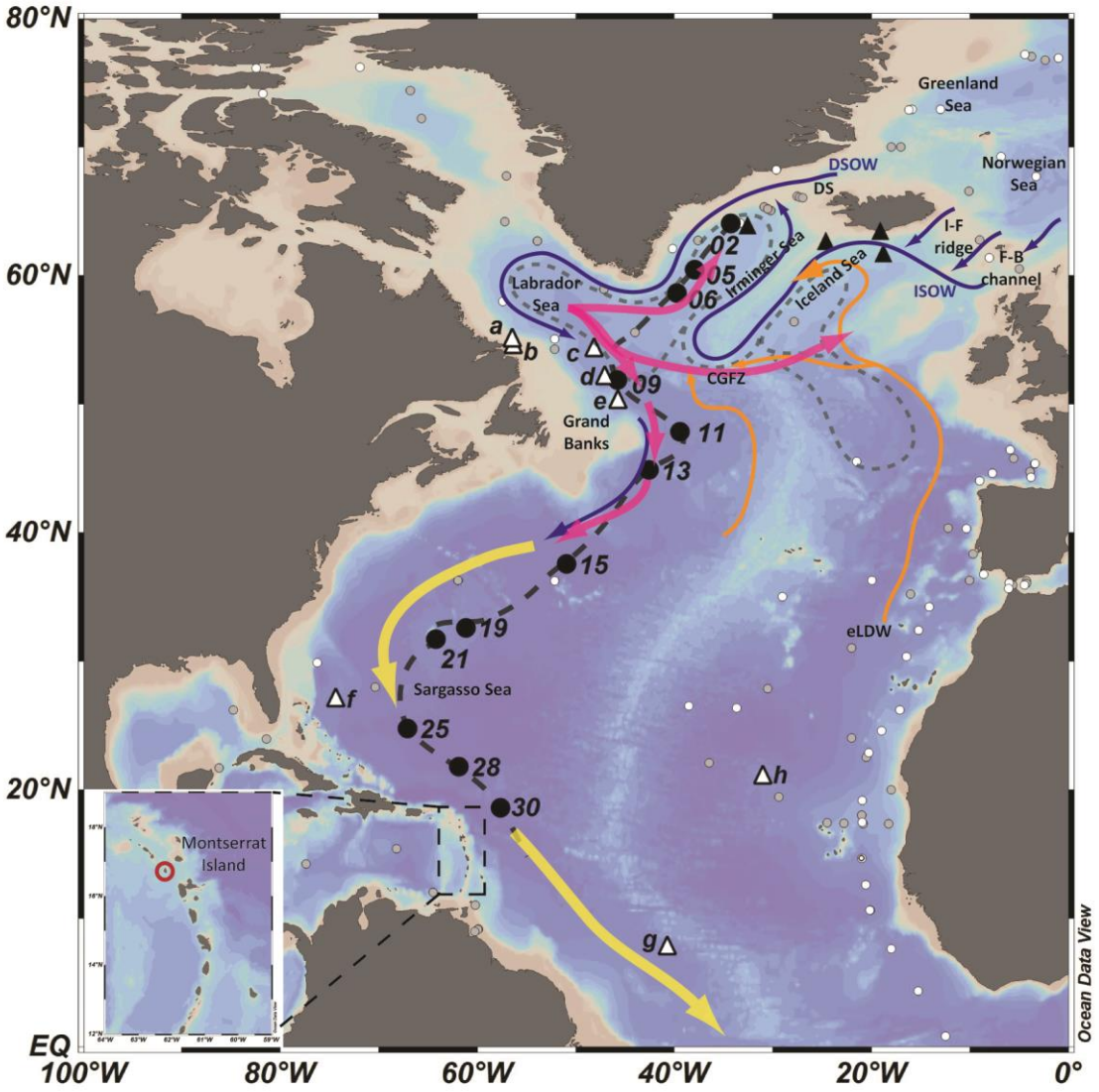
80°N
60°N
40°N
20°N
EQ
100°W
80°W
60°W
40°W
20°W
0°
Greenland Sea
Norwegian Sea
DSOW
DS
I-F ridge
F-B channel
ISOW
Irminger Sea
Iceland Sea
Labrador Sea
CGFZ
Grand Banks
eLDW
Sargasso Sea
Montserrat Island
02
05
06
09
11
13
15
19
21
25
28
30
a
b
c
d
e
f
g
h
Ocean Data View

Fig. 1

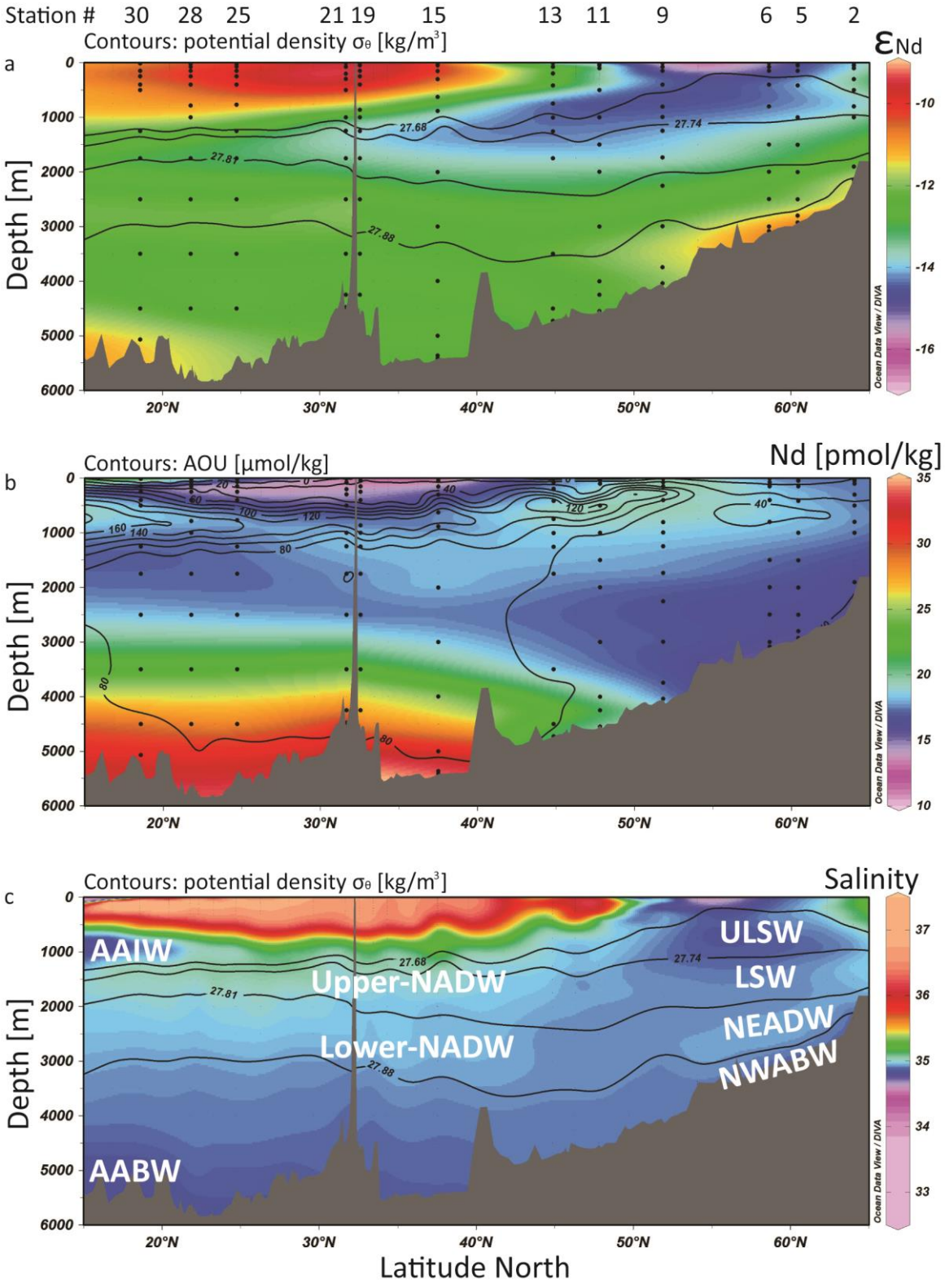
Station # 30 28 25 21 19 15 13 11 9 6 5 2
a
Contours: potential density σθ [kg/m³]
εNd
Depth [m]
27.68
27.74
27.81
27.88
-10
-12
-14
-16
Ocean Data View / DIVA
20°N
30°N
40°N
50°N
60°N
b
Contours: AOU [µmol/kg]
Nd [pmol/kg]
Depth [m]
20
40
60
80
100
120
140
160
35
30
25
20
15
10
c
Contours: potential density σθ [kg/m³]
Salinity
AAIW
Upper-NADW
Lower-NADW
AABW
ULSW
LSW
NEADW
NWABW
37
36
35
34
33
Latitude North

Fig. 2

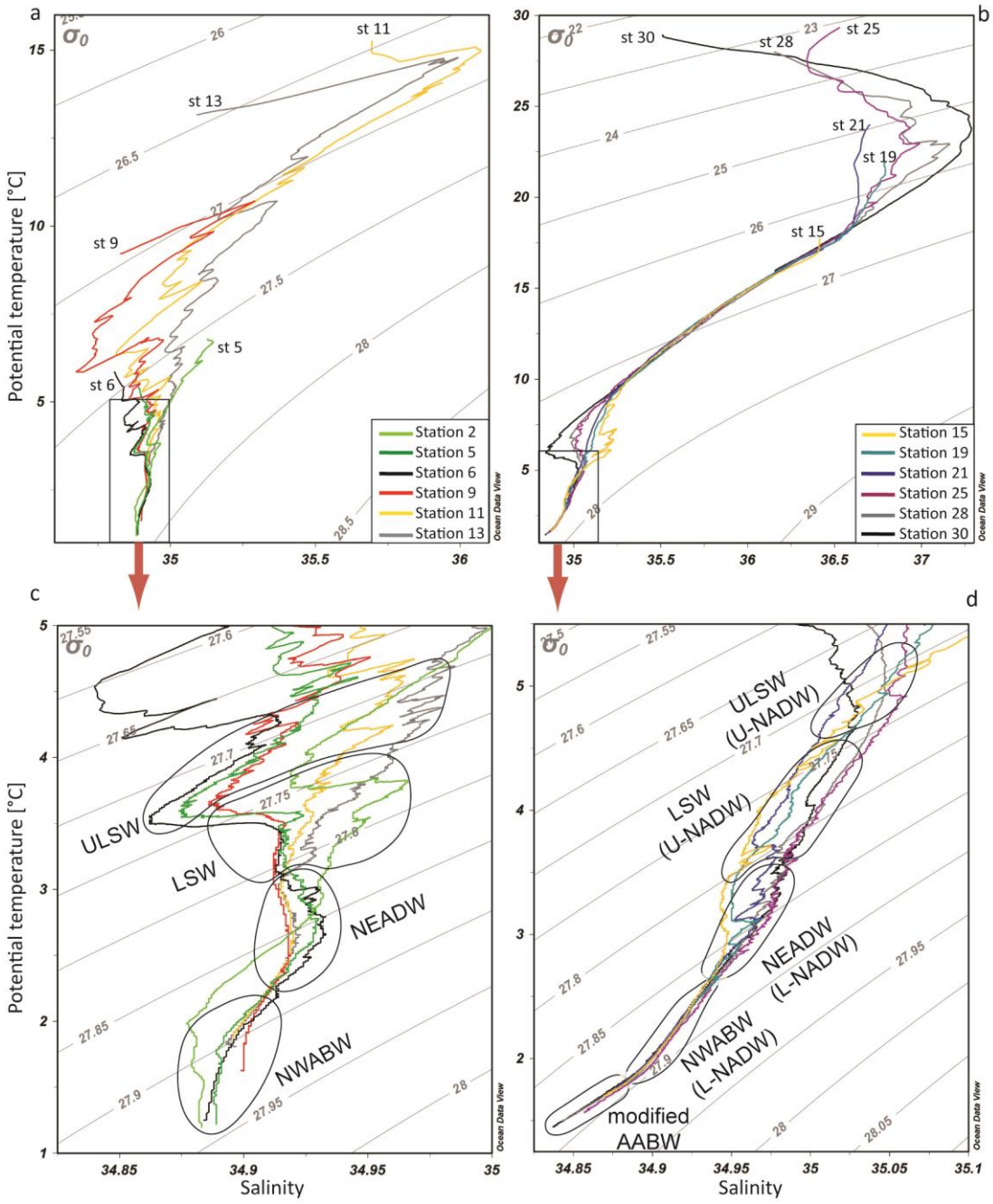
a
b
c
d
Potential temperature [°C]
Salinity
st 11
st 13
st 9
st 5
st 6
st 30
st 28
st 25
st 21
st 19
st 15
Station 2
Station 5
Station 6
Station 9
Station 11
Station 13
Station 15
Station 19
Station 21
Station 25
Station 28
Station 30
ULSW
LSW
NEADW
NWABW
ULSW (U-NADW)
LSW (U-NADW)
NEADW (L-NADW)
NWABW (L-NADW)
modified AABW
Ocean Data View

Fig. 3

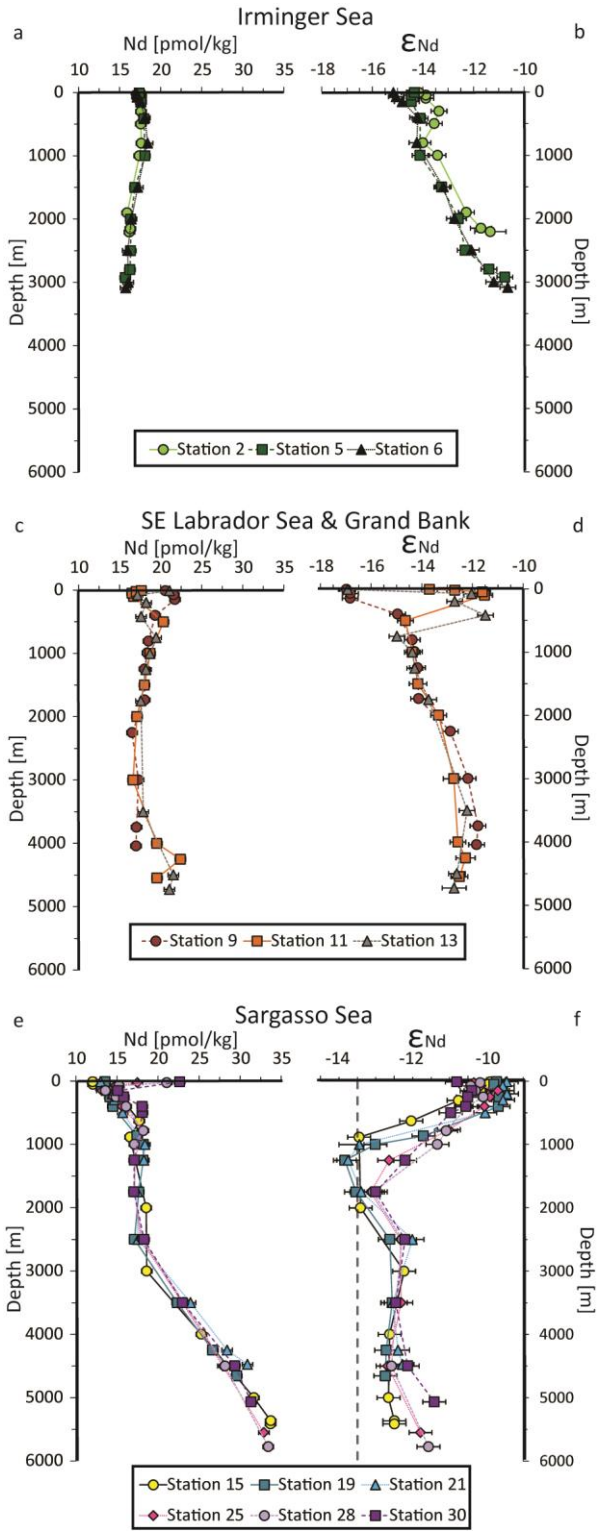
Irminger Sea
a
Nd [pmol/kg]
εNd
b
Depth [m]
Station 2
Station 5
Station 6
SE Labrador Sea & Grand Bank
c
d
Station 9
Station 11
Station 13
Sargasso Sea
e
f
Station 15
Station 19
Station 21
Station 25
Station 28
Station 30

Fig. 4

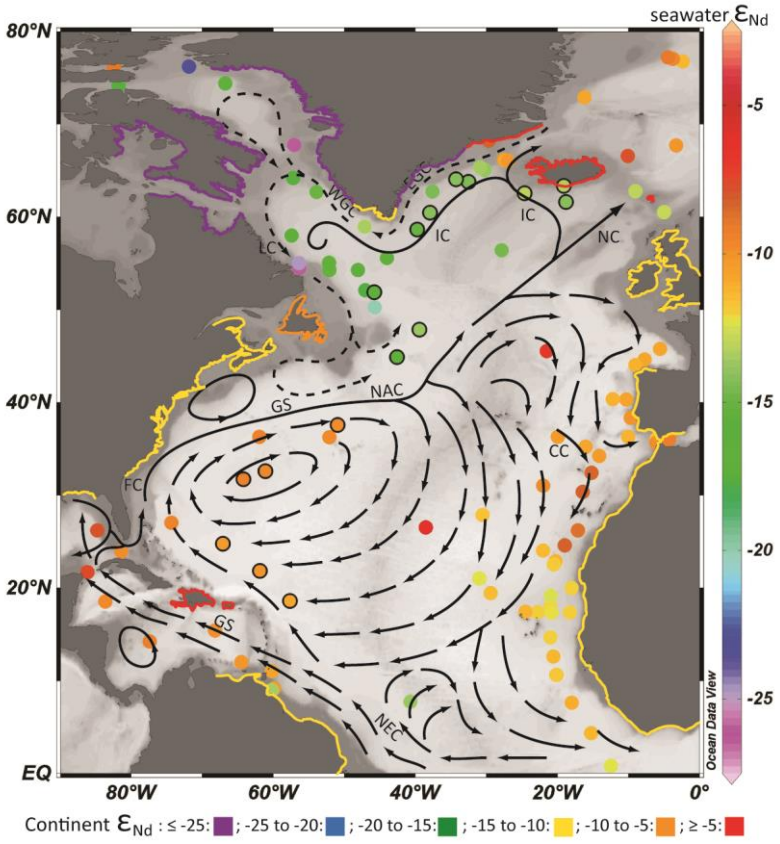
seawater εNd
-5
-10
-15
-20
-25
80°N
60°N
40°N
20°N
EQ
80°W
60°W
40°W
20°W
0°
WGC
EGC
IC
IC
LC
NC
NAC
GS
CC
FC
GS
NEC
Ocean Data View
Continent εNd : ≤ -25: ; -25 to -20: ; -20 to -15: ; -15 to -10: ; -10 to -5: ; ≥ -5:

Fig. 5

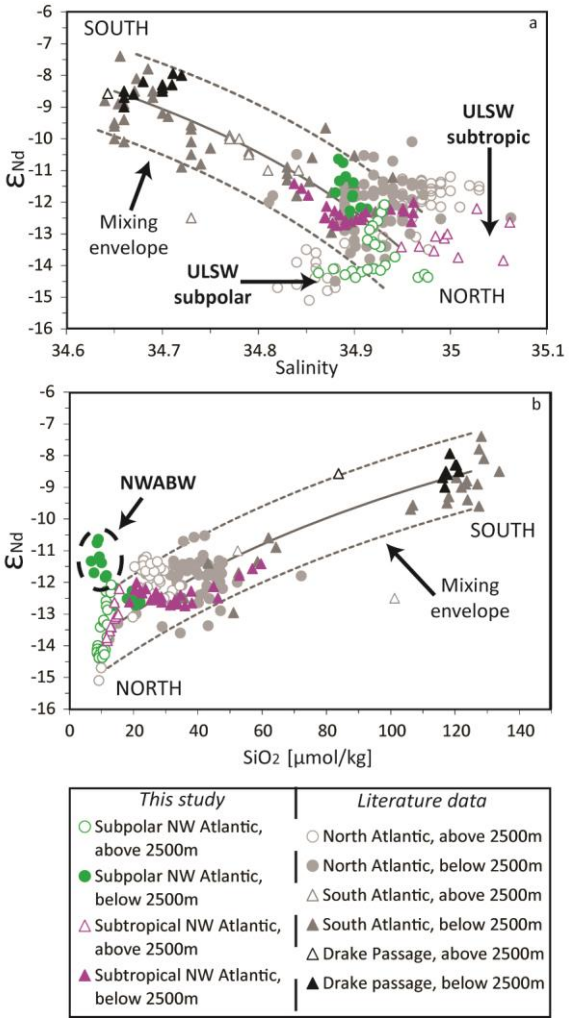
a
SOUTH
ULSW
subtropic
Mixing
envelope
ULSW
subpolar
NORTH
εNd
Salinity
b
NWABW
SOUTH
Mixing
envelope
NORTH
SiO2 [µmol/kg]
This study
Subpolar NW Atlantic, above 2500m
Subpolar NW Atlantic, below 2500m
Subtropical NW Atlantic, above 2500m
Subtropical NW Atlantic, below 2500m
Literature data
North Atlantic, above 2500m
North Atlantic, below 2500m
South Atlantic, above 2500m
South Atlantic, below 2500m
Drake Passage, above 2500m
Drake passage, below 2500m

Fig. 6

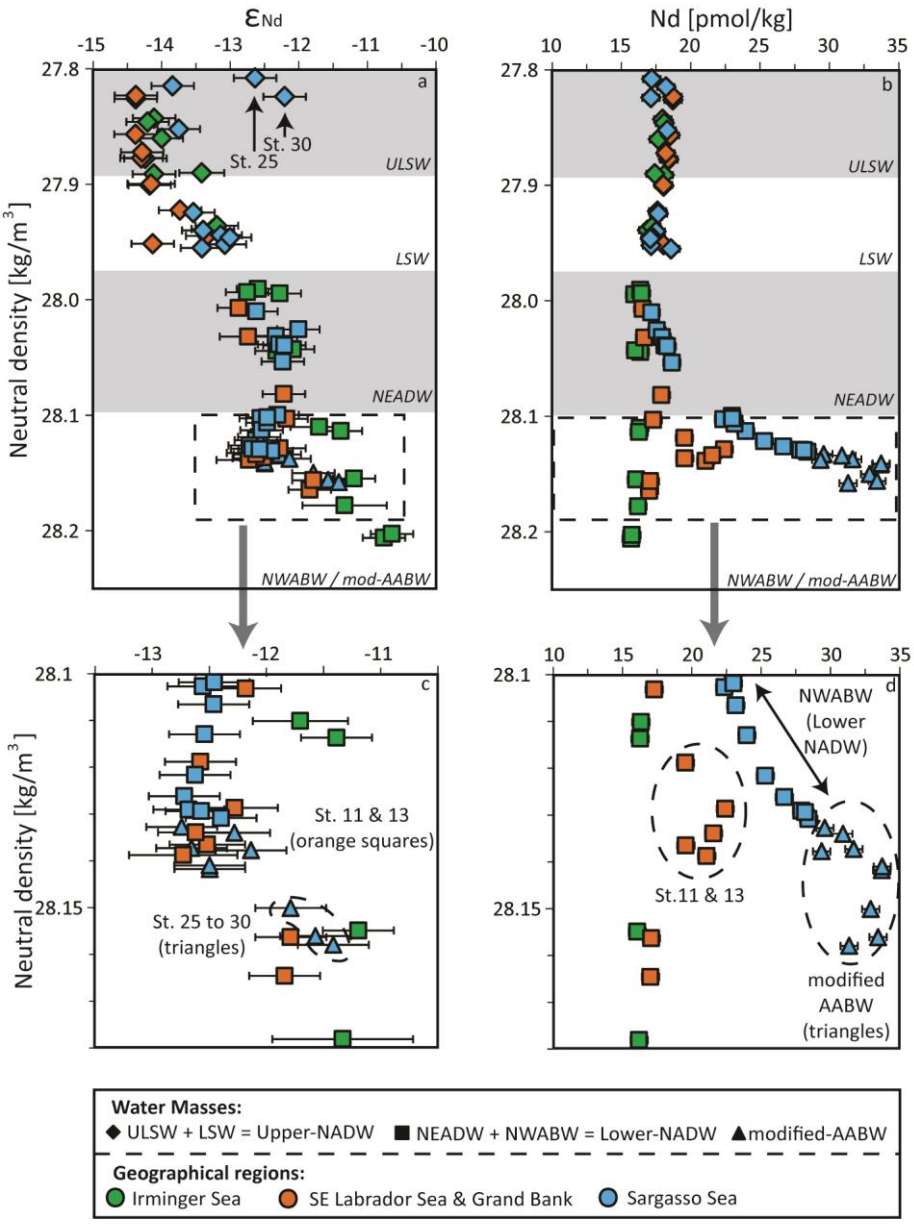
εNd
Nd [pmol/kg]
Neutral density [kg/m3]
a
b
c
d
St. 25
St. 30
ULSW
LSW
NEADW
NWABW / mod-AABW
St. 11 & 13
(orange squares)
St. 25 to 30
(triangles)
NWABW
(Lower
NADW)
St.11 & 13
modified
AABW
(triangles)
Water Masses:
ULSW + LSW = Upper-NADW
NEADW + NWABW = Lower-NADW
modified-AABW
Geographical regions:
Irminger Sea
SE Labrador Sea & Grand Bank
Sargasso Sea

Fig. 7

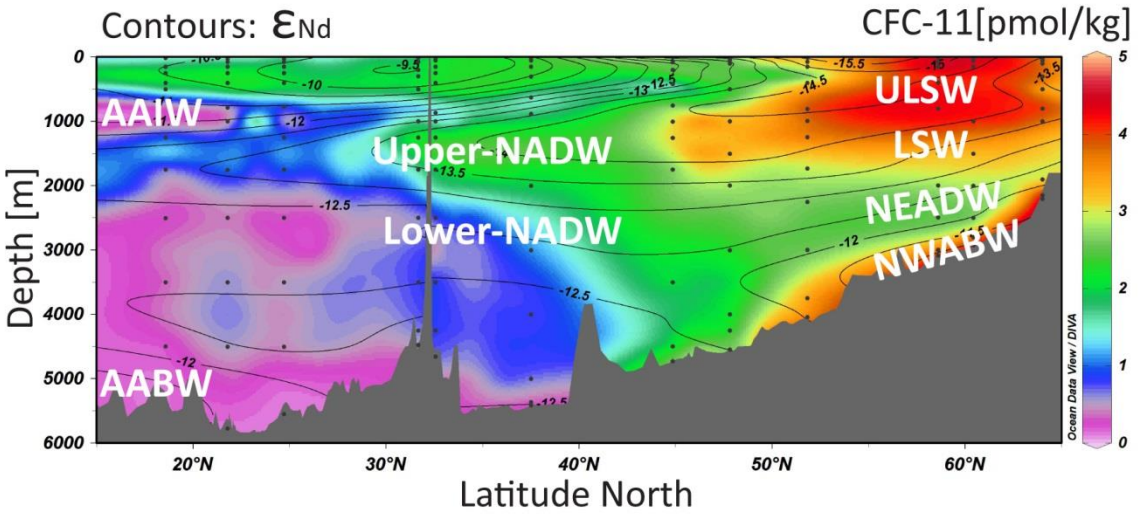
Contours: εNd
CFC-11[pmol/kg]
AAIW
Upper-NADW
Lower-NADW
AABW
ULSW
LSW
NEADW
NWABW
Depth [m]
Latitude North
20°N
30°N
40°N
50°N
60°N
Ocean Data View / DIVA

Fig. 8

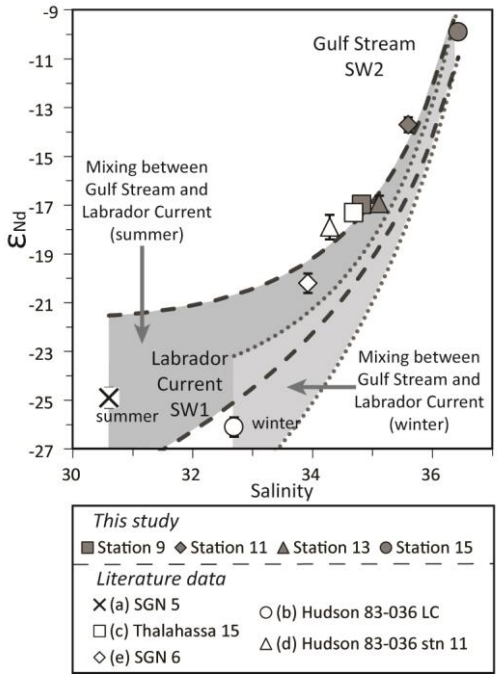
Gulf Stream
SW2
Mixing between
Gulf Stream and
Labrador Current
(summer)
Labrador
Current
SW1
summer
winter
Mixing between
Gulf Stream and
Labrador Current
(winter)
εNd
Salinity
This study
Station 9
Station 11
Station 13
Station 15
Literature data
(a) SGN 5
(b) Hudson 83-036 LC
(c) Thalahassa 15
(d) Hudson 83-036 stn 11
(e) SGN 6

Fig. 9

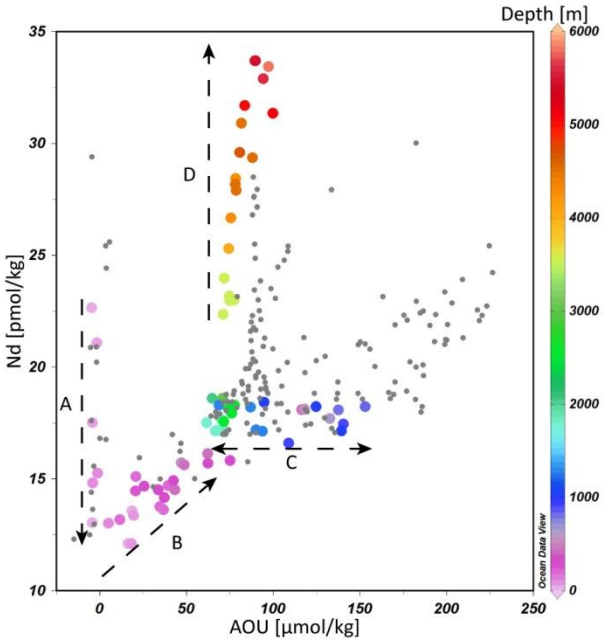
Depth [m]
6000
5000
4000
3000
2000
1000
0
Nd [pmol/kg]
35
30
25
20
15
10
AOU [µmol/kg]
0
50
100
150
200
250
A
B
C
D
Ocean Data View

Fig. 10

Table 1: Neodymium isotopic composition for GEOTRACES reference material from the Bermuda Atlantic Time-Series Study (BATS).

		Analysis date	Sample volume [L]	$^{143}Nd/^{144}Nd$[a]	ε_{Nd}[b]	Internal 2se[c]	External 2sd[d]	Nd [pmol/kg]	Internal 2se[e]
Intercalibration	**BATS 15m**	29/09/2011	10.7	0.5121679	-9.17	0.06	0.19	14.2	0.01
		17/10/2011	7.6	0.5121701	-9.13	0.08	0.13	14.6	0.01
In-house monitoring of sample reproducibility	**BATS 15m**	18/10/2011	9.5	0.5121664	-9.20	0.06	0.13	-	-
		23/11/2011	9	0.5121681	-9.17	0.16	0.16	14.0	0.01
		02/02/2012	5.2	0.5121686	-9.16	0.26	0.08	-	-
		02/02/2012	5	0.5121668	-9.19	0.21	0.08	-	-
Average 2sd BATS 15m				***0.512168***	***-9.17***	***0.05***		***14.3***	***0.6***
Intercalibration	**BATS 2000m**	29/09/2011	10.4	0.5119682	-13.07	0.08	0.19	18.0	0.009
		17/10/2011	7.2	0.5119578	-13.27	0.09	0.13	17.7	0.011
In-house monitoring of sample reproducibility	**BATS 2000m**	28/02/2013	4.9	0.511954	-13.34	0.10	0.14	17.3	0.001
		11/04/2013	4.5	0.511960	-13.23	0.11	0.14	17.3	0.002
		25/04/2013	4.8	0.511973	-12.96	0.08	0.06	17.3	0.002
Average and 2sd BATS 2000m				***0.511963***	***-13.17***	***0.31***		***17.5***	***0.6***

[a] Normalised relative to JNdi value of 0.512115 (Tanaka et al., 2000).

[b] Normalized to JNdi value of 0.512115 (Tanaka et al., 2000) and calculated relative to a CHUR of 0.512638 (Jacobsen and Wasserburg, 1980).

[c] Internal measurement error based on ≤ 360 cycles of static measurements.

[d] External errors are based on the analysis of five standards (JNdi-1) per measurement session.

[e] Internal errors describe the absolute uncertainty and take into account relative uncertainty on weighing of sample and spike, as well as relative uncertainty of TIMS measurements.

Table 2: Location, depth, hydrological properties, nutrient concentration, Nd concentrations and Nd isotopic compositions for the 12 depth profiles collected on GEOTRACES cruise GA02 on the RV *Pelagia* in 2010.

Sample depth [m]	Salinity[a]	Pot. Temp. (Θ) [˚C][a]	Pot. Dens. (σ_θ) [kg/m^3]	Neutral Dens. (γ^n) [kg/m^3]	O_2 [µmol/kg][a]	Phosphate [µmol/kg][b]	Silicate [µmol/kg][b]	Nitrate [µmol/kg][b]	AOU [µmol/kg][c]	CFC-11 [pmol/kg][d]	$^{143}Nd/^{144}Nd$[e]	ε_{Nd}[f]	2se (int.)[g]	Nd [pmol/kg][h]	Water mass
Station 02.3 (2 May 2010; 64.0003˚N – 34.2505˚W; 2215m)															
10	35.131	6.78	27.554	27.657	273.6	0.89	6.37	13.64	22.2	3.84	0.511912	-14.15	0.29	17.6	(sub)surface
50	35.149	6.71	27.579	27.683	268.8	0.91	6.32	13.98	27.6	-	0.511926	-13.88	0.12	17.6	(sub)surface
100	35.148	6.69	27.581	27.687	268.4	0.93	6.35	14.13	28.1	3.82	0.511926	-13.88	0.08	17.6	(sub)surface
302	35.100	6.15	27.616	27.712	269.0	0.99	7.23	15.31	31.6	3.77	0.511953	-13.36	0.29	17.6	(sub)surface
499	35.022	5.26	27.667	27.776	245.4	1.10	9.21	16.67	61.9	3.42	0.511944	-13.55	0.14	17.6	(sub)surface
802	34.932	4.10	27.726	27.860	269.4	1.08	8.88	16.46	47.0	4.04	0.511920	-14.00	0.24	17.7	ULSW
1000	34.927	3.86	27.745	27.890	264.4	1.09	9.69	16.63	53.9	3.79	0.511950	-13.42	0.33	17.4	LSW
1901	34.929	3.02	27.830	27.995	271.3	1.08	11.46	16.31	54.3	2.95	0.512009	-12.28	0.25	15.9	NEADW
2151	34.880	1.85	27.891	28.110	295.7	0.91	7.74	13.67	40.1	4.14	0.512038	-11.70	0.42	16.3	NWABW
2206	34.884	1.26	27.938	28.178	301.6	0.87	6.85	13.06	39.1	4.36	0.512057	-11.33	0.62	16.2	NWABW
Station 05.1 (4 May 2010; 60.4277˚N – 37.9078˚W; 2943m)															
10	34.892	5.39	27.546	27.659	298.5	0.81	4.17	12.10	7.8	4.39	0.511903	-14.34	0.12	17.4	(sub)surface
50	34.913	4.94	27.616	27.737	295.1	0.85	4.66	12.99	14.5	-	0.511897	-14.45	0.12	17.2	(sub)surface
150	34.923	4.58	27.664	27.793	280.6	1.02	7.49	15.55	31.7	-	0.511897	-14.46	0.11	17.6	(sub)surface
417	34.920	4.19	27.705	27.843	269.0	1.08	8.73	16.46	46.4	4.08	0.511915	-14.11	0.10	18.0	ULSW
1001	34.878	3.55	27.738	27.891	273.8	1.08	9.32	16.52	47.1	4.11	0.511915	-14.11	0.13	18.1	ULSW
1502	34.919	3.44	27.782	27.939	267.2	1.10	10.69	16.65	54.8	3.25	0.511959	-13.25	0.09	16.9	LSW
2001	34.924	3.08	27.821	27.991	272.0	1.09	11.52	16.57	53.3	2.89	0.511992	-12.60	0.10	16.4	NEADW
2499	34.928	2.68	27.860	28.044	274.4	1.08	12.91	16.16	54.4	2.65	0.512006	-12.33	0.09	16.4	NEADW
2799	34.899	2.01	27.893	28.114	288.0	0.99	10.11	14.78	46.7	3.65	0.512054	-11.39	0.11	16.3	NWABW
2924	34.888	1.23	27.943	28.206	298.2	0.93	8.71	13.80	43.3	4.07	0.512086	-10.76	0.20	15.7	NWABW

Table 2 (continued)

Sample depth [m]	Salinity[a]	Pot. Temp. (Θ) [˚C][a]	Pot. Dens. (σ_θ) [kg/m^3]	Neutral Dens. (γ^n) [kg/m^3]	O_2 [µmol/kg][a]	Phosphate [µmol/kg][b]	Silicate [µmol/kg][b]	Nitrate [µmol/kg][b]	AOU [µmol/kg][c]	CFC-11 [pmol/kg][d]	$^{143}Nd/^{144}Nd$[e]	ε_{Nd}[f]	2se (int.)[g]	Nd [pmol/kg][h]	Water mass
Station 06.1 (5 May 2010; 58.6027˚N – 39.7064˚W; 3101 m)															
10	34.811	5.84	27.426	27.528	287.5	0.82	4.71	12.01	15.6	4.27	0.511861	-15.17	0.11	17.1	(sub)surface
74	34.839	5.20	27.526	27.638	286.7	0.89	5.27	12.89	21.1	-	0.511866	-15.05	0.12	17.1	(sub)surface
152	34.848	4.27	27.638	27.766	283.4	0.99	7.01	15.04	31.4	-	0.511878	-14.82	0.09	17.6	(sub)surface
399	34.908	4.08	27.707	27.846	268.8	1.06	8.69	16.59	47.5	4.12	0.511910	-14.20	0.12	18.1	ULSW
801	34.863	3.54	27.726	27.878	277.3	1.05	8.74	16.31	43.5	4.27	0.511908	-14.24	0.09	18.4	ULSW
1499	34.914	3.43	27.778	27.936	267.0	1.10	10.74	16.92	55.1	3.23	0.511962	-13.19	0.08	17.2	LSW
1998	34.919	3.03	27.821	27.993	271.8	1.09	11.59	16.52	53.9	2.80	0.511984	-12.75	0.12	16.4	NEADW
2495	34.931	2.71	27.860	28.043	274.2	1.08	13.09	16.45	54.4	2.55	0.512019	-12.08	0.08	16.0	NEADW
2999	34.891	1.66	27.914	28.155	294.3	0.97	9.44	14.68	43.5	3.64	0.512064	-11.20	0.11	16.1	NWABW
3086	34.884	1.25	27.938	28.203	297.8	0.94	9.12	14.14	43.7	3.94	0.512092	-10.64	0.10	15.8	NWABW
Station 09.1 (9 May 2010; 51.8203˚N – 45.7325˚W; 4052 m)															
10	34.819	9.16	26.954	27.026	261.7	0.42	1.85	5.56	19.1	3.40	0.511768	-16.98	0.11	20.6	(sub)surface
75	34.902	8.39	27.141	27.219	253.0	0.70	4.86	9.68	32.6	2.69	0.511776	-16.82	0.09	21.6	(sub)surface
149	34.742	6.83	27.242	27.328	244.4	0.86	6.12	12.54	52.0	-	0.511775	-16.83	0.12	21.8	(sub)surface
400	34.923	4.97	27.621	27.741	231.3	1.13	9.74	17.39	78.2	3.10	0.511871	-14.96	0.14	19.3	(sub)surface
805	34.901	3.96	27.715	27.857	263.6	1.09	9.31	16.81	53.9	3.94	0.511901	-14.38	0.12	18.5	ULSW
993	34.890	3.73	27.730	27.877	267.6	1.09	9.38	16.72	51.8	3.77	0.511905	-14.29	0.12	18.4	ULSW
1247	34.898	3.60	27.749	27.901	267.7	1.10	9.89	16.88	52.9	3.67	0.511911	-14.18	0.13	18.1	LSW
1735	34.914	3.31	27.790	27.952	269.9	1.11	11.26	17.08	53.6	2.92	0.511914	-14.13	0.16	18.1	LSW
2252	34.916	2.91	27.830	28.007	-	1.09	11.95	16.48	-	-	0.511978	-12.87	0.11	16.5	NEADW
2997	34.907	2.14	27.890	28.103	277.8	1.06	14.29	15.97	55.9	2.52	0.512014	-12.18	0.14	17.3	NWABW
3745	34.898	1.70	27.917	28.156	287.9	0.98	11.61	14.78	50.3	3.41	0.512034	-11.79	0.12	17.1	NWABW
4041	34.898	1.64	27.922	28.165	290.5	0.98	11.22	14.71	48.6	3.58	0.512031	-11.84	0.12	17.0	NWABW

Table 2 (continued)

Sample depth [m]	Salinity[a]	Pot. Temp. (Θ) [˚C][a]	Pot. Dens. (σ_θ) [kg/m^3]	Neutral Dens. (γ^n) [kg/m^3]	O_2 [µmol/kg][a]	Phosphate [µmol/kg][b]	Silicate [µmol/kg][b]	Nitrate [µmol/kg][b]	AOU [µmol/kg][c]	CFC-11 [pmol/kg][d]	$^{143}Nd/^{144}Nd$[e]	ε_{Nd}[f]	2se (int.)[g]	Nd [pmol/kg][h]	Water mass
Station 11.3 (11 May 2010; 47.7996˚N – 39.4001˚W; 4570 m)															
9	35.596	15.20	26.419	26.466	259.5	0.03	0.05	0.36	-13.6	2.65	0.511936	-13.70	0.13	17.7	(sub)surface
23	35.886	14.87	26.689	26.745	237.9	0.06	0.20	2.66	9.3	-	0.511987	-12.70	0.13	17.0	(sub)surface
50	36.026	15.06	26.754	26.810	219.9	0.25	1.72	3.97	26.1	-	0.512043	-11.61	0.10	16.5	(sub)surface
101	36.004	14.56	26.848	26.904	212.6	0.38	2.58	6.30	36.0	2.51	0.512047	-11.53	0.11	16.7	(sub)surface
502	35.003	8.07	27.270	27.356	160.8	1.28	11.07	21.02	127.0	2.27	0.511887	-14.65	0.13	20.4	(sub)surface
1001	34.966	4.60	27.697	27.826	243.4	1.12	10.34	17.17	69.2	3.21	0.511901	-14.38	0.16	18.7	ULSW
1501	34.927	3.80	27.752	27.900	261.1	1.13	10.63	17.06	58.1	3.26	0.511912	-14.15	0.35	18.0	LSW
1998	34.922	3.41	27.786	27.945	264.7	1.13	11.81	17.37	57.9	-	0.511954	-13.34	0.25	17.1	LSW
3000	34.919	2.74	27.847	28.032	271.8	1.10	13.90	16.69	57.0	2.24	0.511985	-12.74	0.41	16.7	NEADW
4000	34.899	1.99	27.896	28.119	275.5	1.12	19.92	16.66	60.5	2.10	0.511993	-12.58	0.23	19.5	NWABW
4251	34.895	1.90	27.900	28.129	275.2	1.12	19.59	16.64	61.8	2.19	0.512009	-12.28	0.38	22.4	NWABW
4547	34.895	1.84	27.905	28.137	278.9	1.09	18.03	16.33	58.9	2.54	0.511996	-12.52	0.33	19.6	NWABW
Station 13.1 (13 May 2010; 44.8442˚N – 42.5260˚W; 4751 m)															
10	35.112	13.21	26.440	26.489	270.2	0.04	0.18	0.00	-13.3	3.05	0.511770	-16.93	0.13	21.1	(sub)surface
77	35.934	14.69	26.766	26.820	220.5	0.26	1.44	4.04	27.5	-	0.512021	-12.04	0.18	17.2	(sub)surface
198	35.654	13.23	26.859	26.916	199.0	0.58	3.79	9.40	57.1	2.55	0.511987	-12.71	0.11	18.3	(sub)surface
418	35.313	10.24	27.160	27.228	126.9	1.39	11.86	22.32	146.7	1.48	0.512049	-11.49	0.10	17.6	(sub)surface
750	34.992	5.61	27.598	27.712	210.8	1.23	11.58	18.90	94.1	2.68	0.511870	-14.98	0.15	19.5	(sub)surface
1003	34.977	4.68	27.696	27.823	240.1	1.15	10.85	17.80	71.9	2.93	0.511901	-14.38	0.18	18.7	ULSW
1256	34.973	4.28	27.738	27.872	248.7	1.15	11.01	17.63	66.5	3.11	0.511906	-14.28	0.15	18.2	ULSW
1750	34.942	3.70	27.774	27.923	258.9	1.14	11.78	17.58	61.2	2.62	0.511934	-13.73	0.22	17.6	LSW
3501	34.913	2.34	27.879	28.082	272.6	1.11	17.20	16.82	60.0	2.04	0.512012	-12.22	0.13	17.9	NEADW
4499	34.892	1.85	27.903	28.134	272.8	1.15	22.10	17.09	64.9	2.00	0.511991	-12.62	0.13	21.6	NWABW
4726	34.893	1.82	27.906	28.139	276.3	1.11	20.65	16.72	61.9	2.53	0.511986	-12.73	0.47	21.1	NWABW

Table 2 (continued)

Sample depth [m]	Salinity[a]	Pot. Temp. (Θ) [˚C][a]	Pot. Dens. (σ_θ) [kg/m^3]	Neutral Dens. (γ^n) [kg/m^3]	O_2 [µmol/ kg][a]	Phosphate [µmol/ kg][b]	Silicate [µmol/ kg][b]	Nitrate [µmol/ kg][b]	AOU [µmol/kg][c]	CFC-11 [pmol/ kg][d]	$^{143}Nd/^{144}Nd$[e]	ε_{Nd}[f]	2se (int.)[g]	Nd [pmol/kg][h]	Water mass
Station 15.6 (19 May 2010; 37.5164˚N – 50.8906˚W; 5441 m)															
11	36.428	17.79	26.424	26.465	216.3	0.02	0.17	0.28	16.4	2.29	0.512131	-9.90	0.14	12.1	WNACW
52	36.428	17.76	26.429	26.470	214.5	0.03	0.18	0.34	18.3	-	0.512128	-9.96	0.11	12.1	WNACW
153	36.385	16.84	26.621	26.665	197.7	0.34	2.05	6.36	39.4	-	0.512117	-10.16	0.14	14.7	WNACW
304	36.152	15.74	26.699	26.746	180.3	0.51	3.04	8.90	62.4	2.30	0.512087	-10.75	0.13	15.7	WNACW
629	35.310	9.88	27.218	27.287	143.3	1.37	11.75	21.78	132.6	1.55	0.512021	-12.04	0.12	17.7	WNACW
885	35.202	6.97	27.591	27.675	186.1	-	-	-	108.9	-	0.511948	-13.45	0.11	16.6	WNACW
2003	34.949	3.49	27.801	27.955	257.2	1.16	13.10	17.68	64.7	1.97	0.511950	-13.41	0.13	18.6	uNADW (LSW)
3002	34.937	2.66	27.870	28.054	258.5	1.20	20.40	18.15	70.9	-	0.512011	-12.23	0.12	18.6	mNADW (NEADW)
3999	34.896	1.96	27.898	28.122	262.0	1.26	28.8	18.68	74.3	0.77	0.511991	-12.62	0.10	25.3	lNADW (NWABW)
5001	34.877	1.76	27.900	28.137	255.5	1.37	38.19	20.12	83.5	0.65	0.511989	-12.66	0.12	31.7	AABW
5364	34.870	1.71	27.899	28.141	250.4	-	-	-	89.5	-	0.511997	-12.50	0.12	33.7	AABW
5414	34.869	1.70	27.899	28.142	250.3	1.47	46.3	21.54	89.8	0.28	0.511997	-12.50	0.11	33.7	AABW
Station 19.1 (23 May 2010; 32.5514˚N – 61.0986˚W; 4683 m)															
10	36.795	21.96	25.598	25.614	196.4	0.01	0.61	0.00	18.6	1.99	0.512139	-9.72	0.10	13.6	ESW
50	36.762	20.72	25.917	25.940	200.4	0.01	0.61	0.01	19.5	-	0.512136	-9.80	0.10	13.4	ESW
149	36.627	18.76	26.331	26.365	193.6	0.05	0.75	1.60	34.6	-	0.512148	-9.56	0.09	13.8	STMW (WNACW)
251	36.588	18.33	26.411	26.446	193.1	0.10	0.94	2.61	37.1	-	0.512143	-9.66	0.08	14.2	STMW (WNACW)
401	36.541	17.88	26.487	26.524	189.1	0.18	1.29	3.89	43.3	2.19	0.512142	-9.67	0.08	14.5	STMW (WNACW)
866	35.261	9.47	27.250	27.323	138.2	1.40	12.29	22.39	140.5	1.36	0.512038	-11.71	0.13	17.5	WNACW
1001	35.120	7.25	27.482	27.571	168.6	1.39	13.12	21.60	124.8	1.51	0.511971	-13.01	0.08	18.2	WNACW
1251	35.055	5.18	27.701	27.815	221.4	1.22	11.90	18.71	86.9	2.18	0.511929	-13.84	0.12	18.2	uNADW (ULSW)
1750	34.983	3.92	27.784	27.925	248.4	1.17	12.60	17.93	69.9	1.93	0.511944	-13.54	0.07	17.7	uNADW (LSW)
2500	34.959	3.10	27.847	28.010	254.2	1.21	18.77	18.30	71.2	0.76	0.511991	-12.62	0.11	17.2	mNADW (NEADW)
3501	34.907	2.14	27.891	28.103	263.0	1.22	25.35	18.30	71.2	0.84	0.511994	-12.56	0.07	22.4	lNADW (NWABW)
4250	34.890	1.89	27.898	28.126	261.4	1.28	31.51	19.00	75.7	0.81	0.511986	-12.72	0.09	26.7	lNADW (NWABW)
4655	34.881	1.81	27.899	28.133	257.5	1.33	36.01	19.75	80.7	0.71	0.511985	-12.74	0.09	29.6	AABW

Table 2 (continued)

Sample depth [m]	Salinity[a]	Pot. Temp. (Θ) [˚C][a]	Pot. Dens. (σ_θ) [kg/m^3]	Neutral Dens. (γ^n) [kg/m^3]	O_2 [µmol/ kg][a]	Phosphate [µmol/ kg][b]	Silicate [µmol/ kg][b]	Nitrate [µmol/ kg][b]	AOU [µmol/kg][c]	CFC-11 [pmol/ kg][d]	$^{143}Nd/^{144}Nd$[e]	ε_{Nd}[f]	2se (int.)[g]	Nd [pmol/kg][h]	Water mass
Station 21.2 (BATS; 13 June 2010; 31.6669˚N – 64.1664˚W; 4567 m)															
9	36.699	23.78	24.995	25.000	212.7	0.02	0.43	0.01	-4.4	1.68	0.512154	-9.45	0.16	13.0	ESW
75	36.613	18.70	26.335	26.369	223.4	0.01	0.46	0.19	5.0	1.96	0.512148	-9.56	0.09	13.0	STMW (WNACW)
201	36.566	18.05	26.464	26.500	210.8	0.14	1.10	3.17	20.6	1.98	0.512154	-9.44	0.18	14.5	STMW (WNACW)
297	36.521	17.74	26.507	26.543	207.3	0.20	1.34	4.06	25.7	2.01	0.512149	-9.55	0.13	14.7	STMW (WNACW)
500	36.298	16.54	26.626	26.666	192.0	0.41	2.39	7.46	46.9	2.03	0.512124	-10.03	0.12	15.7	-*
1001	35.071	6.03	27.608	27.711	207.1	1.34	12.78	20.55	94.8	1.70	0.511949	-13.44	0.56	18.4	*uNADW*
1249	35.008	4.64	27.726	27.852	243.7	1.20	11.67	18.42	68.7	2.18	0.511933	-13.75	0.13	18.3	uNADW (ULSW)
1749	34.968	3.71	27.793	27.940	258.4	1.16	12.95	17.97	61.5	1.62	0.511951	-13.39	0.11	17.5	uNADW (LSW)
2501	34.962	2.99	27.859	28.026	254.7	1.24	20.98	18.66	71.5	0.60	0.512022	-12.01	0.26	17.6	mNADW (NEADW)
3500	34.902	2.04	27.895	28.113	263.3	1.24	27.10	18.44	71.8	0.78	0.511995	-12.54	0.23	24.0	lNADW (NWABW)
4249	34.885	1.84	27.899	28.131	259.3	1.31	34.61	19.69	78.3	0.63	0.512003	-12.40	0.27	28.4	lNADW (NWABW)
4474	34.877	1.77	27.898	28.134	256.0	1.39	40.15	20.67	81.7	0.53	0.512009	-12.28	0.23	30.9	AABW
Station 25.1 (17 June 2010; 24.7147˚N – 67.0728˚W; 5575 m)															
25	36.570	25.87	24.262	24.258	205.4	0.01	0.98	0.00	-4.2	-	0.512108	-10.34	0.14	17.5	ESW
73	36.900	23.31	25.288	25.297	213.9	0.01	0.79	0.00	-4.1	1.86	0.512118	-10.14	0.11	14.8	ESW
150	36.725	20.19	26.031	26.057	210.6	0.01	0.74	0.01	11.5	-	0.512141	-9.69	0.10	13.2	WNACW
251	36.578	18.38	26.391	26.426	196.3	0.15	1.31	3.67	33.7	-	0.512130	-9.91	0.12	14.5	WNACW
400	36.405	17.19	26.552	26.592	187.0	0.34	2.10	6.58	48.7	2.02	0.512123	-10.05	0.11	15.6	WNACW
767	35.289	9.86	27.206	27.276	138.6	1.49	12.99	24.19	137.6	0.88	0.512073	-11.02	0.10	18.1	AAIW
1250	35.062	5.27	27.696	27.808	217.4	1.31	14.10	20.47	90.2	0.95	0.511990	-12.64	0.12	17.2	uNADW (ULSW)
1751	34.994	3.82	27.803	27.944	251.1	1.19	14.14	18.33	68.0	0.98	0.511964	-13.14	0.08	17.2	uNADW (LSW)
2500	34.961	2.94	27.863	28.031	250.6	1.25	22.69	19.17	76.1	0.32	0.512006	-12.34	0.09	17.9	mNADW (NEADW)
3499	34.912	2.19	27.891	28.100	258.8	1.25	27.05	18.84	75.0	0.51	0.512007	-12.31	0.11	23.0	lNADW (NWABW)
4500	34.890	1.87	27.900	28.129	258.8	1.32	33.85	19.58	78.7	0.42	0.511988	-12.68	0.08	27.9	lNADW (NWABW)
5551	34.852	1.57	27.896	28.150	247.1	1.53	52.95	22.51	94.3	0.11	0.512034	-11.79	0.11	32.9	AABW

Table 2 (continued)

Sample depth [m]	Salinity[a]	Pot. Temp. (Θ) [˚C][a]	Pot. Dens. (σ_θ) [kg/m^3]	Neutral Dens. (γ^n) [kg/m^3]	O_2 [µmol/kg][a]	Phosphate [µmol/kg][b]	Silicate [µmol/kg][b]	Nitrate [µmol/kg][b]	AOU [µmol/kg][c]	CFC-11 [pmol/kg][d]	$^{143}Nd/^{144}Nd$[e]	ε_{Nd}[f]	2se (int.)[g]	Nd [pmol/kg][h]	Water mass
Station 28.1 (20 June 2010; 21.7764˚N – 61.8438˚W; 5795 m)															
25	36.218	27.72	23.404	23.393	197.1	0.01	1.06	0.00	-1.6	1.49	0.512117	-10.17	0.10	21.1	ESW
74	36.887	23.51	25.218	25.227	210.2	0.01	0.75	0.00	-1.1	-	0.512103	-10.43	0.09	15.3	ESW
150	36.889	20.84	25.979	26.002	182.5	0.03	0.78	1.06	36.8	-	0.512110	-10.30	0.11	13.6	ESW
251	36.575	18.23	26.424	26.460	188.2	0.20	1.41	4.39	42.5	-	0.512121	-10.09	0.12	14.9	WNACW
401	36.229	16.16	26.660	26.703	178.5	0.49	2.87	8.94	62.2	2.21	0.512099	-10.52	0.10	16.1	WNACW
785	35.106	8.27	27.321	27.406	133.5	1.71	16.53	27.03	153.0	0.54	0.512069	-11.09	0.09	18.2	AAIW
998	34.995	6.30	27.514	27.621	160.8	1.71	18.94	26.36	139.3	0.36	0.512057	-11.33	0.10	17.1	AAIW
1752	34.984	3.70	27.808	27.952	253.3	1.19	14.49	18.31	66.7	0.96	0.511968	-13.08	0.10	17.1	uNADW (LSW)
2501	34.952	2.84	27.866	28.039	253.3	1.24	22.08	18.69	74.2	0.38	0.512008	-12.29	0.09	18.1	mNADW (NEADW)
3499	34.907	2.11	27.893	28.107	259.8	1.25	27.23	18.65	74.7	0.55	0.511999	-12.46	0.09	23.2	lNADW (NWABW)
4501	34.891	1.87	27.901	28.129	259.4	1.30	32.88	19.24	78.1	0.54	0.511994	-12.57	0.09	28.2	lNADW (NWABW)
5775	34.845	1.50	27.896	28.156	244.9	1.59	56.98	23.29	97.4	0.12	0.512045	-11.57	0.09	33.4	AABW
Station 30.2 (22 June 2010; 18.5724˚N – 57.6121˚W; 5280 m)															
11	35.503	29.02	22.437	22.413	196.8	0.01	0.44	0.00	-4.7	1.43	0.512084	-10.80	0.18	22.7	ESW
152	37.224	22.90	25.654	25.669	190.1	0.02	0.60	0.25	20.9	-	0.512105	-10.40	0.23	15.1	ESW
249	36.626	18.45	26.409	26.445	154.5	0.41	2.05	7.83	75.2	-	0.512099	-10.51	0.19	15.8	WNACW
402	35.914	14.36	26.821	26.871	133.5	0.95	5.36	16.55	116.5	1.99	0.512097	-10.56	0.21	18.1	WNACW
499	35.650	12.40	27.021	27.077	142.7	1.11	7.46	18.84	118.1	1.76	0.512076	-10.97	0.32	18.1	WNACW
1250	35.028	4.97	27.704	27.824	216.0	1.37	15.59	21.03	93.8	0.90	0.512012	-12.21	0.30	17.1	uNADW (ULSW)
1749	34.997	3.81	27.806	27.946	247.4	1.23	15.28	18.86	71.7	0.61	0.511971	-13.00	0.12	17.1	uNADW (LSW)
2502	34.951	2.83	27.866	28.039	249.9	1.27	23.77	19.30	77.7	0.27	0.512012	-12.21	0.15	18.3	mNADW (NEADW)
3500	34.909	2.16	27.891	28.102	256.7	1.27	28.65	19.06	77.4	0.31	0.511999	-12.46	0.09	23.0	lNADW (NWABW)
4499	34.871	1.73	27.896	28.138	250.7	1.45	44.89	21.38	88.1	0.18	0.512016	-12.13	0.10	29.4	AABW
5067	34.837	1.45	27.892	28.158	242.0	1.61	59.67	23.75	99.8	0.13	0.512053	-11.42	0.11	31.4	AABW

[a] Hydrological properties measured on board the RV *Pelagia* using CTD-systems equipped with a Seabird SBE-9+ underwater unit, a SBE 3+ thermometer, a SBE4-conductivity sensor, a SBE 5T underwater pump, a Chelsea Aquatracka fluorometer and a Wetlabs CStar-transmissiometer.

[b] Nutrients concentrations measured on board the RV *Pelagia* within 3 hours after sampling on a Seal Analytical QuAAtro Autoanalyser connected to an autosampler; determined by calorimetry.

[c] Apparent oxygen utilisation (AOU) derived by *Ocean Data View*-program (Schlitzer, 2012).

[d] Chlorofluorocarbon (CFC) were collected into 100 mL glass ampoules and sealed off after a CFC free headspace of pure nitrogen had been applied. The determination of CFC concentration was performed at the University of Bremen by purge and trap sample pre-treatment followed by gas chromatography separation on a capillary column and electron capture detection.

[e] Normalised relative to JNdi value of 0.512115 (Tanaka et al., 2000) using five runs of JNdi.

[f] ε_{Nd} values were calculated relative to a CHUR of 0.512638 (Jacobsen and Wasserburg, 1980). External errors are the two sigma standard deviations derived from repeat analyses of seawater samples (n = 5) reported in Table 1 (31 ppm).

[g] Internal measurement error based on ≤ 360 cycles of static measurements.

[h] Internal errors describe the absolute uncertainty and take into account relative uncertainty on weighing of sample and spike, as well as relative uncertainty of TIMS measurements. At a maximum they represent 0.03% of the samples concentrations and are therefore not reported. The external 2 sigma error is based on repeat analyses of in-house seawater (n = 5) presented in Table 1 and is 0.6 pmol/kg. The external error is what is quoted in figures and text.

[*] According to the hydrological characteristics used to define the different water masses, this sample could not be assigned to a specific water mass.

Table 3: Abbreviations used for water masses and surface water currents.

Water masses	
AABW	Antarctic Bottom Water
AAIW	Antarctic Intermediate Water
AW	Atlantic Water
DSOW	Denmark Strait Overflow Water
EDW	Eighteen Degrees Water (also called STMW)
ESW	Equatorial Surface Water
ISOW	Iceland Scotland Overflow Water
LDW	Lower Deep Water
LSW	Labrador Sea Water
MOW	Mediterranean Outflow Water
NADW	North Atlantic Deep Water
NEADW	North East Atlantic Deep Water
NWABW	North West Atlantic Bottom Water
OW	Overflow Waters
SPMW	Subpolar Mode Water
STMW	Subtropical Mode Water (also called EDW)
ULSW	Upper Labrador Sea Water
WNACW	Western North Atlantic Central Water
Ocean currents	
DWBC	Deep Western Boundary Current
EGC	East Greenland Current
IC	Irminger Current
LC	Labrador Current
NAC	North Atlantic Current
WGC	Western Greenland Current

Table 4: Location, collection date, Nd isotopic composition and concentration for surface seawater samples collected in the vicinity of Iceland during the 2010 Eyjafjallajökull volcano eruption.

Sample	Latitude [˚N]	Longitude [˚W]	Sampling date	$^{143}Nd/^{144}Nd$[a]	ε_{Nd}[b]	2se (int.)[c]	Nd [pmol/kg][d]
Pelagia FISH	61.57	18.77	30/04/2010	0.511912	-14.15	0.14	17.3
Pelagia FISH	62.51	24.58	01/05/2010	0.511971	-13.02	0.16	16.9
Pelagia FISH	63.73	32.51	02/05/2010	0.511900	-14.40	0.24	17.1
D-350	63.30	19.05	08/05/2010	0.511958	-13.27	0.13	18.2

[a] Normalised relative to JNdi value of 0.512115 (Tanaka et al. 2000) using five runs of JNdi.

[b] ε_{Nd} values were calculated relative to a CHUR of 0.512638 (Jacobsen and Wasserburg 1980). External errors are the two sigma standard deviations derived from repeat analyses of in-house seawater samples (n = 5) reported in Table 1 (31 ppm).

[c] Internal measurement error based on ≤ 360 cycles of static measurements.

[d] External errors are the two sigma standard deviations based on repeat analyses of in-house seawater samples (n = 5) reported in Table 1 (0.6 pmol/kg).

Note that cruise on the RV *Pelagia* did not sample the ash plume, while the cruise on the RRS *Discovery* (D-350) did (Achterberg et al., 2013).